ACS APPLIED NANO MATERIALS

www.acsanm.org

Article

Immunochemical Design of Antibody-Gated Indicator Delivery (gAID) Systems Based on Mesoporous Silica Nanoparticles

Estela Climent,* Michael G. Weller, Ramón Martínez-Máñez, and Knut Rurack

Cite This: *ACS Appl. Nano Mater.* 2022, 5, 626–641

Read Online

ACCESS | Metrics & More | Article Recommendations | Supporting Information

ABSTRACT: In this work, the optimization of the immunochemical response of antibody-gated indicator delivery (gAID) systems prepared with mesoporous silica nanoparticles has been studied along various lines of system tailoring, targeting the peroxide-type explosive TATP as an exemplary analyte. The mechanism of detection of these gAID systems relies on a displacement of an antibody "cap" bound to hapten derivatives anchored to the surface of a porous hybrid material, allowing the indicator cargo stored in the mesopores to escape and massively amplify the analyte-related signal. Since our aim was to obtain gAID systems with the best possible response in terms of sensitivity, selectivity, and assay time, sera obtained from different immunization boosts were screened, the influence of auxiliary reagents was assessed, structural hapten modification (hapten heterology) was investigated, and various indicator dyes and host materials were tested. Considering that highly selective and sensitive immunological responses are best obtained with high-affinity antibodies which, however, could possess rather slow dissociation constants, leading to slow responses, the main challenge was to optimize the immunochemical recognition system for a rapid response while maintaining a high sensitivity and selectivity. The best performance was observed by grafting a slightly mismatching (heterologous) hapten to the surface of the nanoparticles in combination with high-affinity antibodies as "caps", yielding for the first time gAID nanomaterials for which the response time could be improved from hours to <5 min. The materials showed favorable detection limits in the lower ppb range and discriminated TATP well against H_2O_2 and other explosives. Further optimization led to straightforward integration of the materials into a lateral flow assay without further treatment or conditioning of the test strips while still guaranteeing remarkably fast overall assay times.

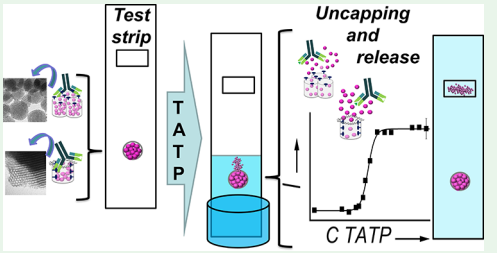

KEYWORDS: *antibody-gated indicator delivery systems, signal amplification, immunochemical response optimization, test strip analysis, TATP, explosives detection, heterologous hapten*

1. INTRODUCTION

The design of stimuli-responsive materials for controlled delivery applications is a vibrant area of research,[1−3] spanning from cancer therapy to corrosion prevention.[4,5] Hybrid (bio)organic−inorganic materials play a key role in the field, involving metal−organic frameworks as well as (organo)silicas and ranging from particles to membranes.[6−9] Especially, in connection with mesoporous silica nanoparticles as host materials, many different control functions have been realized, including also various examples of reversibility or degradability on demand.[10−13] Particularly appealing are materials that incorporate (bio)chemical entities that can act as supramolecular "gates" because they allow cargo delivery control through a wide variety of specific (bio)molecular stimuli.[14−16] Until today, the majority of the systems have been developed for the considerably slow release of drug molecules. However, in recent years, the use of such hybrids in analytical applications especially became very attractive.[17,18] For such an approach, indicator or reporter molecules are loaded as cargo into the pores, and an analyte-specific combination of "gatekeeping" chemistry is attached at the pore openings. This gatekeeping chemistry usually comprises a small molecule that is covalently attached to the outer surface of the porous particle and a "cap", usually a bulky (bio)macromolecule or small nanoparticle that is non-covalently bound to the former. In the case of this immunochemical system, the "gatekeepers" consist of hapten molecules, which can be bound by the antibody. These haptens are structurally related to the immunogen, which had been used for the generation of selective antibodies. This ensemble is designed in such a way that an analyte molecule present in a sample can successfully compete with the gatekeeper, thus leading to an uncapping of the pore and subsequent release of its colored, fluorescent, or redox-active cargo. As only a few analyte molecules are required to uncap a pore, which then releases a much larger number of indicators, massive chemical signal amplification can result.[19,20] The basic architectural and operational principles of

Received: October 14, 2021
Accepted: December 9, 2021
Published: December 30, 2021

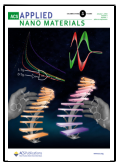

such systems are illustrated in Scheme S1, Supporting Information. Obviously, in the field of analytical chemistry, where such an approach is especially suitable for (bio)sensing applications with rather low-cost (miniaturized) devices or quick tests, the delivery has to be specific and fast. Our interest in the development of gated material-based sensing systems[21−24] motivated us to explore the possibility of immunochemical gating because an architecture that uses a hapten derivative as the gatekeeper and an antibody as the cap harbors the prospect of a modular, adaptable and even multiplexed platform.[25−30] However, keeping in mind the essential difference between controlled drug release (often over many hours) and sensing or rapid testing, in which a user or a usage scenario commonly tolerates response times of maximal 5 min, the optimization procedures are supposedly different for materials for either type of application. In addition, the selectivity requirements are much higher in analytical applications. However, to the best of our knowledge, no studies have yet been reported that deal with design aspects that allow for the turning of a slow drug release system into a fast indicator delivery system. Therefore, since most examples on gated indicator-releasing particles reported in the literature so far show a rather slow kinetics of ≥20 min until a stable signal is reached,[20,31,32] we evaluated several parameters along which such materials can be modified toward improved response times and higher efficiency. The latter is important to achieve low limits of detection in rather simple analytical test formats.

Antibody-gated indicator delivery (gAID) systems consist of a mesoporous support functionalized at the pore outlets with a hapten derivative that interacts sufficiently strong with an antibody to close the pores. The opening mechanism is based on the inhibition of the rebinding of the antibody to the surface-bound hapten in the dynamic dissociation/association situation. Only the rebinding (association step) can be inhibited. The interaction between antibody cap and hapten gatekeeper is noncovalent. Hence, antibody and hapten should at best be chosen in a way that the affinity of the antibody is low enough so that fast off-rates are guaranteed, allowing for rapid opening. However, fast off-rates often come along with lower affinity constants and hence poor analytical sensitivity and leaching issues. This conflict of objectives needs to be addressed.

Our first examples of gAID systems also suffered from the problem of many delivery systems for analytical applications mentioned above, i.e., slow response kinetics of 60 min and longer.[25,26] As such a behavior is certainly not ideal for a rapid test such as as a lateral flow assay (LFA), we embarked on a series of optimization studies. LFAs are perhaps the most promising format for the use of gAID materials as they allow in a uniquely straightforward way to separate the reporters released out of opened pores from those still confined in closed pores of the host material after contact with a sample.[28] Whereas the mesoporous particles are too large to travel along the strip with the flow, released indicators can do so. Material optimization has been addressed in the context of drug delivery, yet many works focused on the impact of surface functionalization on the performance and fate of such hybrid systems, in particular, in the context of interactions at the material−cell level.[33] Structure−performance relationships have also been addressed for mesoporous materials employed in (bio)analytical chemistry, yet here, utmost works compare only systems with different gatekeeping chemistries or reporters as cargo and remain silent about material chemistry tailoring aspects; only pore size and/or pore connectivity in relation to size exclusion and mass transport have been frequently studied.[34]

Optimization of the gating and indication mechanism, however, does not only depend on pore morphology, but parameters such as the localization of grafted functional groups or molecules, the grafting density, linker length and polarity, the loading/grafting sequence(s), or affinity tuning, and indicator−scaffold interactions play important roles as well.[29] This is of particular importance when biomolecular recognition is involved, as biomacromolecules often have specific demands with respect to buffers or avoidance of nonspecific adsorption. Recent optimization studies by us on grafting sequence and localization in combination with different pore sizes provided a better understanding of the system, especially with respect to the size of antibodies and their structural subunits in relation to the pore size of the porous silica materials.[29,35] In another work, we assessed the influence of the chemical nature of the indicator dye on the loading and release efficiency into and from mesoporous silica nanoparticles.[36] However, because of the use of a commercially available antibody,[37,38,a] these studies could not efficiently elucidate the potential that lies in the tuning of the gatekeeping immunochemistry as such. The latter became possible within the framework of BAM's program to generate antibodies against the most widely used explosives.[30,39−42] Here, we thus report on a detailed optimization study of a gAID system for the detection of triacetone triperoxide (TATP). This analyte is an organic peroxide that has become an illicit explosive of choice in improvised explosive devices (IEDs) for criminal and terrorist activities due to its straightforward synthesis using readily available household chemicals as precursors—acetone and hydrogen peroxide. TATP is difficult to target with conventional recognition chemistry because it lacks functional groups for classical noncovalent binding and is neither particularly polar nor non-polar. In addition, lacking nitrogen-containing groups or substituents, TATP detection can also not be accomplished with conventional explosives detection devices targeting trinitrotoluene (TNT), tetryl, hexogen (RDX), octogen (HMX), or other nitro-containing substances. Its detection as a peroxide is usually aggravated by hydrogen peroxide, its precursor, and decomposition product, potentially inducing false positives.[43,44] Immunochemical TATP tests are therefore one of the few methods to directly detect this hazard.

Whereas we have already reported the best performing system,[27] the present contribution discusses the first in-depth study of the various immunochemical considerations of such gAID systems, essentially sketching a workflow to gAID systems with an optimized response in terms of sensitivity, selectivity, and assay time. The effect of the different antibody fractions or haptens employed as well as buffer conditions was assessed, along with the component ratios and the use of an organic co-solvent, to accelerate kinetics. By grafting a slightly altered variant of the hapten (heterology concept) used during the immunization of the animals on the surface of the sensing materials and combining it with high-affinity antibodies as caps as well as an organic co-solvent, the response time could be reduced from >60 to 5 min while reaching sensitivities in the lower ppb range with an excellent selectivity. Integration with test strips finally yielded a lateral flow assay, which offers straightforward handheld operation with a simple fluorescence readout.

https://doi.org/10.1021/acsanm.1c03417
ACS Appl. Nano Mater. 2022, 5, 626−641

2. EXPERIMENTAL SECTION

2.1. General Techniques. Powder-X-ray diffraction (P-XRD), thermogravimetric analysis (TGA), elemental analysis, transmission electron microscopy (TEM), N_2 adsorption−desorption isotherm measurements, nuclear magnetic resonance (NMR), UV−visible absorption, and fluorescence spectroscopy techniques were employed to characterize the synthesized materials and test their behavior toward TATP, other explosives, and related peroxides (see SI for more details).

2.2. Reagents. Chemicals and solvents were purchased from Sigma-Aldrich, Merck, and J.T. Baker in the highest quality available. Acetone (Pico grade) was supplied by LGC Standards. The buffers and solutions were prepared with ultrapure reagent water, which was obtained by running demineralized water (by ion exchange) through a Milli-Q ultrapure water purification system (Millipore Synthesis A10). The protein bovine serum albumin (BSA, for immunogen synthesis, fraction V, receptor grade, lyophilized) was purchased from Serva. Phosphate-buffered saline (PBS; 70 mM Na_2HPO_4, 10 mM KH_2PO_4, 145 mM NaCl, pH 7.4) and PBS with 0.05% BSA were used for capping, controlled release experiments, interference, and competition studies. Fluorescein (FLU, **1**), rhodamine 101 chloride salt (Rh101, **2**), sulforhodamine B sodium salt (SRB, **3**), and rhodamine B chloride salt (RhB, **4**) were employed as releasable indicator cargo, loaded in either ethanol (EtOH), acetonitrile (ACN), or PBS buffer. The common explosives nitropenta (PETN), TNT, RDX, and HMX were obtained from BAM Division 2.5 *Conformity Assessment Explosives and Pyrotechnics*. 1,4,7,10-Tetraoxacyclododecane (12-crown-4, 98%), 1,4,7,10,13,16-hexaoxacyclooctadecane (18-crown-6, 99.5%), and nitroguanidine (NG, containing ca. 25% water) were purchased from Sigma Aldrich. High flow nitrocellulose membranes were obtained from Millipore (HF135).

Safety Note! Only highly qualified personnel should work with TATP, other peroxides, or commercial explosives, and safety precautions must be strictly adhered to avoid hazardous situations. Furthermore, only small amounts of less than 100 mg should be synthesized and handled. TATP and other peroxides can detonate spontaneously, particularly under impact, friction, static electricity, or temperature changes.

2.3. Syntheses of Compounds. *2.3.1. Synthesis of TATP, Cyclic Triperoxides, and Other Explosives.* The synthesis of triacetone triperoxide (TATP) was carried out employing a procedure described earlier by us.[39] The other cyclic triperoxides tri-butanone triperoxide (but-TP), tri-2-pentanone triperoxide (2-pent-TP), and tri-3-pentanone triperoxide (3-pent-TP) were prepared following the same procedure as for TATP synthesis, employing butanone, 2-pentanone, and 3-pentanone instead of acetone.[27] Other common explosives such as DADP (diacetone diperoxide) and hexamethylene triperoxide diamine (HMTD) were also prepared following procedures described previously.[45,46]

2.3.2. Synthesis of Haptens I and II and Hapten Derivatives III and IV. Haptens **I** and **II** were prepared following the procedure described previously for TATP. For the preparation of hapten **I**, we used acetone, 7-oxooctanoic acid (7-oxo), hydrogen peroxide, and sulfuric acid, whereas for hapten **II**, we used butanone instead of acetone.

The hapten derivative **III** was obtained through an amidation reaction between **I** and the alkoxysilane derivative (3-aminopropyl)-triethoxysilane (APTES) via a modified active ester method.[47] In a first step, anhydrous THF solutions of *N*-hydroxysuccinimide (NHS, 24.85 mg in 0.2456 mL) and *N*,*N*′-dicyclohexylcarbodiimide (DCC, 15.17 mg in 0.0868 mL) were prepared. Then, 0.025 mL of each solution (0.021 mmol of NHS and 0.021 mmol of DCC) were added to a solution of hapten **I** (8 mg, 0.018 mmol) in anhydrous THF (0.25 mL). The mixture was stirred at room temperature for 5 h, and the white solid formed (dicyclohexylurea) was removed by centrifugation. Stirring was repeated for another 15 h at room temperature, and the white solid formed was also removed by centrifugation. In a second step, APTES (4.3 μL, 0.018 mmol) was added to the solution, and the reaction mixture was stirred for 24 h at room temperature. The solvent was evaporated under reduced pressure to give a yellow sticky oil (**III**, 8.5 mg, 0.016 mmol, yield 89.8%). ^{1}H NMR ($CDCl_3$): δ = 0.63 ((t, 2 H, $-CH_2-$Si−), 1.23 (t, 9 H, SiO$-CH_2-CH_3$) 1.35 (m, 8 H, $CH_2-CH_2-CH_2-CH_2-CH_2-$CO−NH−), 1.39 (s, 3 H, ($CH_3$) −C− CH_2). 1.61 (s, 12 H, $2(CH_3)_2$−C−) 1.66 (m, 2 H, −NH$-CH_2-CH_2-CH_2-$Si−), 1.92 (m, 2 H, $-CH_2-CH_2-CH_2-CH_2-CH_2-$CO−NH−), 3.24 (t, 2H, −NH$-CH_2-CH_2-CH_2-$Si−), 3.81 (s, 6H, CH_3-CH_2-O−Si−). ^{13}C NMR ($CDCl_3$): 7.7, 18.3, 18.6, 21.3, 22.8, 23.7, 24.9, 25.3, 25.6, 29.4, 33.8, 36.8, 41.8, 58.5, 107.4, 109.3, 173.1. Exact mass (M + 1) 526.305; found 526.354.

The hapten derivative **IV** was obtained using the same procedure as described for **III** and reported earlier by us.[27]

2.3.3. Antibodies. The polyclonal antibodies for TATP were obtained by Walter et al.[40] For immunization, hapten **I** was covalently attached through its carboxylic acid moiety to the lysine residues of BSA, using a modified active-ester method. A mean conjugation ratio of 14 hapten molecules per BSA was thus achieved. The TATP−BSA conjugate was employed to immunize two 9−12-week-old (2−2.5 kg) rabbits with subcutaneous injections, and 11 different sera of each rabbit were obtained. Sera were stored at 8 °C containing 0.1% (w/v) sodium azide. These sera were directly used to evaluate the titre and affinity maturation of the hapten-specific antibodies via ELISA. Affinity constants for the polyclonal TATP antibodies were also estimated.

Considering the apparent affinity constants of different boosts (see Table S2, SI), we decided to test sera nos. 4, 5, 8, and 11 in combination with our materials during this study.

2.4. Syntheses of Materials. *2.4.1. Synthesis of MCM-41- and SBA-15-Type Mesoporous Silica Nano- and Microparticles.* Mesoporous nanoparticles of Mobil Composition of Matter-(MCM-)-41-type were synthesized according to an adapted literature procedure,[22,48,49] yielding as-synthesized MCM-41 particles (**S1**). Removal of the templating surfactant by calcination resulted in **S2**. Santa Barbara Amorphous-(SBA)-15-type mesoporous silica particles were also synthesized by an adapted literature method,[50,51] yielding as-synthesized SBA-15 (**S3**). Detailed descriptions are given in Section S1, SI.

2.4.2. Synthesis of $\mathbf{S2.1_E.1}$. **S2** (560 mg) and FLU (cargo **1**, 150 mg, 0.8 mmol g^{-1} solid) were suspended in ethanol (50 mL). The suspension was refluxed (100 °C) in azeotropic distillation, collecting 10 mL in a Dean-Stark apparatus to remove adsorbed water. Thereafter, the suspension was stirred for 24 h at 37 °C to achieve maximum loading of FLU into the pores of the MCM-41 scaffold. Afterward, the solid was filtered off and dried at 40 °C for 12 h, yielding $\mathbf{S2.1_E}$; the subscript "E" denotes loading of **1** into **S2** in ethanol. Next, 56 mg of $\mathbf{S2.1_E}$ were suspended in 2 mL of a solution of hapten derivative **III** (0.018 mmol, 0.32 mmol g^{-1} solid) in acetonitrile, and the final mixture was stirred for 17 h at room temperature. The solid was centrifuged (10 min at 9500 rpm), washed with ACN (1 mL), and isolated by centrifugation again. Finally, material $\mathbf{S2.1_E.1}$ was dried at 35 °C in a vacuum for 12 h.

2.4.3. Synthesis of $\mathbf{S2.2_B.1}$. This material was obtained following a similar procedure as for $\mathbf{S2.1_E.1}$ by suspending 5 mg of **S2** in a solution of PBS (subscript "B", 1.5 mL) containing 1.5 mg Rh101 (cargo **2**, 0.57 mmol g^{-1} solid). The suspension was stirred for 24 h at room temperature before the addition of 0.2 mL of a solution of hapten derivative **III** (1.8 μmol, 0.36 mmol g^{-1} solid) in ACN. After condensation during stirring for 17 h at room temperature, the material was processed as $\mathbf{S2.1_E.1}$ above, yielding $\mathbf{S2.2_B.1}$.

2.4.4. Synthesis of $\mathbf{S2.2_B.2}$. A total of 150 mg of **S2** were suspended in a solution of PBS buffer (13 mL) containing 44.0 mg Rh101 (0.56 mmol g^{-1} solid). The suspension was stirred for 24 h at room temperature before the addition of hapten derivative **IV** (65 mg, 0.12 mmol, 0.8 mmol g^{-1} solid) in 0.5 mL of THF. The final mixture was stirred for 5.5 h at room temperature. The resulting material $\mathbf{S2.2_B.2}$ was centrifuged (10 min at 9500 rpm), washed with PBS buffer (1 mL), isolated by centrifugation, and dried at 35 °C in a vacuum for 12 h.

2.4.5. Synthesis of $\mathbf{S2.3_A.2}$. To load a maximum amount of dye into an MCM-41 scaffolding, a solution of SRB (cargo **3**, 1 mmol L^{-1})

https://doi.org/10.1021/acsanm.1c03417
ACS Appl. Nano Mater. 2022, 5, 626−641

was prepared in ACN (subscript "A").[36] Then, a portion of this solution (44 mL) was added to a suspension of **S2** (55 mg), obtaining a dye concentration of 0.8 mmol g^{-1} solid. The suspension was stirred for 24 h at room temperature. Subsequently, 6 mL of the suspension was removed, centrifuged (10 min at 6000 rpm), and dried at 40 °C for 12 h to estimate the content of dye inside of the pores. The rest of the suspension (38 mL) was centrifuged (10 min at 6000 rpm) and concentrated in a final volume of 1.5 mL before 0.1 mL of a solution of hapten derivative **IV** (0.04 mmol) in THF was added. The resulting suspension was stirred for 17 h at room temperature and centrifuged (10 min at 6000 rpm), and material **S2.3$_A$.2** was washed with ACN (0.75 mL), isolated by centrifugation, and dried at 35 °C in a vacuum for 12 h.

*2.4.6. Synthesis of **S4.2$_B$.1**.* To obtain material **S4.2$_B$.1**, 1.25 g of **S1** was suspended in 50 mL of acetonitrile, and 1.094 mL of n-propyltrimethoxysilane (5 mmol g^{-1} solid) was added to passivate the external surface of MCM-41 with propyl chains. This functionalization blocks the majority of the reactive surface silanol groups. The suspension was stirred for 5.5 h at room temperature before the solid was filtered off, washed with distilled water and acetone, and dried at 40 °C for 1 h. Subsequently, the surfactant was removed by HCl/EtOH extraction. A total of 1.25 g of the solid previously prepared was suspended in 125 mL of HCl (1 M) in EtOH, and the suspension was stirred at 100 °C for 15 h. The solid was filtered off, washed with water until neutral pH, and dried at 60 °C for 12 h, yielding an MCM-41 material with propyl groups anchored on the external surface, **S4**. To anchor the hapten derivative **III** onto the inner walls of the pores of **S4**, 75 mg of this material was suspended in 1.5 mL of a solution of 9 mg of **III** (0.23 mmol g^{-1} solid) in ACN, and the mixture was stirred for 17 h at room temperature. After centrifugation (10 min at 9500 rpm), the material **S4.0.1** was washed with ACN (1 mL) and isolated by centrifugation again (note that the intermediate zero "0" indicates that the pores have not yet been loaded with cargo). In the final step, 75 mg of **S4.0.1** was suspended in 4 mL of PBS containing 18.06 mg of Rh101 (cargo **2**, 0.46 mmol g^{-1} solid). The suspension was stirred for 24 h to load the dye into the pores, yielding **S4.2$_B$.1**, which was subsequently centrifuged (10 min at 9500 rpm) and dried at 35 °C in a vacuum for 12 h.

*2.4.7. Synthesis of **S5.2$_A$.2**.* Material **S5.2$_A$.2** was basically prepared in similar steps as **S4.2$_B$.1** yet using SBA-15 as a host material. For external surface functionalization, 1.25 g of **S3** was suspended in 40 mL of acetonitrile, 1.094 mL of n-propyltrimethoxysilane (5 mmol g^{-1} solid) was added, and the suspension was stirred for 5.5 h at room temperature before filtering off the solid, washing it with acetonitrile and Milli-Q water, and drying at 40 °C for 1 h. The template was removed by extraction after suspending the material containing propyl groups in 100 mL EtOH (abs) containing 0.8 mL HCl (37%) and stirring at 80 °C for 17 h. The material was filtered and washed with water and EtOH until neutral pH and dried at 60 °C overnight in an oven, yielding **S5**. In a next step, 80 mg of **S5** was suspended in 1.5 mL of acetonitrile containing 30 mg of hapten derivative **IV** (0.054 mmol, 0.68 mmol g^{-1} solid) to anchor **IV** on the inner walls of **S5**. This mixture was stirred for 16 h at room temperature before **S5.0.2** was centrifuged (10 min at 9500 rpm), washed with ACN (1 mL) and isolated by centrifugation. In the final step, 25 mg of **S5.0.2** were suspended in 1 mL of ACN containing 10 mg of Rh101 (cargo **2**, 0.75 mmol g^{-1} solid). The suspension was stirred for 24 h, loading the pores with the dye. **S5.2$_A$.2** was then centrifuged (10 min at 9500 rpm) and dried at 35 °C in a vacuum for 12 h.

*2.4.8. Synthesis of **S5.2$_B$.2**.* This material was obtained according to the same procedure as used for **S5.2$_A$.2** but employing PBS buffer instead of ACN for dye loading. Thus, 25 mg of **S5.0.2** was suspended in 10 mL of PBS containing 10 mg of Rh101 (0.75 mmol g^{-1} solid), and the suspension was stirred for 24 h, centrifuged (10 min at 9500 rpm), and dried at 35 °C in a vacuum for 12 h, yielding **S5.2$_B$.2**.

*2.4.9. Synthesis of **S5.4$_A$.2**.* **S5.4$_A$.2** was also prepared in analogy to **S5.2$_A$.2**, only employing RhB (cargo **4**) instead of Rh101. For this purpose, 3.5 mg of **S5.0.2** was suspended in 0.5 mL of ACN containing 2.3 mg RhB (4.8 μmol). The suspension was stirred for 24 h, centrifuged (10 min at 9500 rpm), and dried at 35 °C in a vacuum for 12 h, yielding **S5.4$_A$.2**.

*2.4.10. Synthesis of **S5.4$_B$.2**.* **S5.4$_B$.2** was synthesized in the same way as **S5.4$_A$.2**, only loading RhB in PBS buffer. Therefore, 3.5 mg of solid **S5.0.2** was suspended in 0.5 mL of PBS containing 2.3 mg of RhB (4.8 μmol), stirred for 24 h, centrifuged (10 min at 9500 rpm), and dried at 35 °C in a vacuum for 12 h, resulting in **S5.4$_B$.2**.

*2.4.11. Synthesis of **S5.3$_A$.2**.* Again, as in the case of **S5.4$_A$.2**, 30 mg of **S5.0.2** was suspended in 24 mL of a solution of SRB in ACN (1 mM) before stirring the mixture for 24 h to load the pores with the dye. After centrifugation (10 min at 9500 rpm) and drying at 35 °C in a vacuum for 12 h, **S5.3$_A$.2** was obtained.

2.5. Characterization of Materials. The materials were characterized using standard techniques. The structure of the MCM-41 and SBA-15 materials was confirmed by powder X-ray diffraction (P-XRD), transmission electron microscopy (TEM), and N_2 adsorption−desorption measurements. P-XRD showed the typical hexagonal array of these mesoporous materials (see Section S2, SI, including Figures S1 and S3). The reflection peaks found for all materials proved that the loading with a dye and the functionalization followed by biomacromolecular capping had no detrimental effect on the structure of the materials. The TEM images also showed the typical hexagonal porosity of mesoporous MCM-41 and SBA-15 and the change of appearance of the material's surface because of chemical functionalization and biomacromolecular capping (see Figure 1).

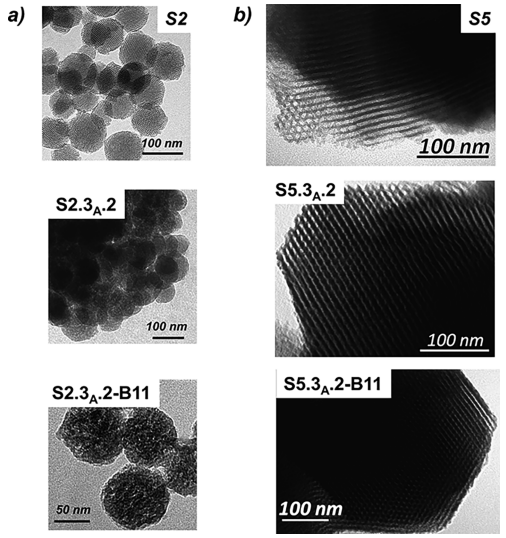

Figure 1. (a) TEM images of materials **S2**, **S2.3$_A$.2**, and **S2.3$_A$.2-B11**, showing the typical hexagonal porosity of the mesoporous MCM-41 matrix. (b) TEM images of materials **S5**, **S5.3$_A$.2**, and **S5.3$_A$.2-B11** showing the typical hexagonal porosity of the mesoporous SBA-15 matrix.

N_2 adsorption−desorption measurements revealed typical curves for mesoporous solids consisting of an adsorption step at intermediate P/P_0 values (0.25−0.4) corresponding to a type IV isotherm, in which the observed step indicated nitrogen condensation inside the mesopores (see Figures S2 and S4). Using Barrett−Joyner−Halenda (BJH) and Brunauer−Emmett−Teller (BET) models, the corresponding values of pore size, pore volume, and specific surface area of the materials were estimated (see Section 3.2 and Section S2, SI for more details). Finally, the content of hapten derivatives **III** and **IV** propyl chains as passivating groups and the different dyes employed in the materials was determined by elemental analysis and thermogravimetric studies (see Table S1 for more details).

2.6. Capping and Optimization of Materials. *2.6.1. General Optimization of the Capping Step.* In general, the amounts of antibody, bovine serum albumin (BSA), and the different sera evaluated were optimized to yield maximum capping while using a

https://doi.org/10.1021/acsanm.1c03417
ACS Appl. Nano Mater. 2022, 5, 626−641

minimum amount of substance. Optimization studies were performed with material **S2.1$_E$.1** and the polyclonal TATP antibodies of serum **B5**. From the experiments reported below, the materials prepared in PBS buffer containing 0.05% BSA, 200 ppm of FLU, and **B5** in a dilution 1/100 showed the best performance.

*2.6.2. Synthesis and Optimization of **S2.1$_E$.1-B5**.* The initial gated material **S2.1$_E$.1-B5** was obtained by weighing 1.5 mg **S2.1$_E$.1** and suspending it in 3 mL PBS (80 mM) containing 200 ppm FLU (to avoid losses of FLU from the pores) and 0.05% BSA. A fraction of 300 μL of this suspension (0.5 mg mL^{-1}) was then spiked with 3 μL of **B5** at a dilution of 1/100 (v/v %). The suspension was mixed in a carousel at room temperature for 1 h. Afterward, the suspension was centrifuged, and the resulting material was washed with 300 μL of PBS containing 0.05% BSA and twice with 300 μL PBS for 1 min to remove dye from any mesopore that was not properly capped. The material was separated by centrifugation and resuspended in 300 μL of PBS to evaluate the dye release as a function of time through absorbance and fluorescence measurements, recording the absorbance, centered at 490 nm, or the emission of FLU, centered at 535 nm, upon excitation at 490 nm using a microplate reader.

To optimize the capping efficiency with respect to the use of BSA and amount of serum, this experiment was repeated in the absence of BSA as well as in the presence of different amounts of serum **B5** (3, 1.5, 0.75, 0.6, 0.3, and 0 μL equivalent to the corresponding **B5** dilutions of 1/100, 1/200, 1/400, 1/500 1/1000, and no serum).

*2.6.3. General Synthesis of the Antibody-Capped Materials **S2.2$_B$.1-Bi (i = 4, 5, 8), S2.2$_B$.2-Bi (i = 4, 8, 11), S2.3$_A$.2-B11, and S4.2$_B$.1-B11**.* The hybrid materials were obtained in a similar way as **S2.1$_E$.1-B5**. A total of 1.5 mg **S2.2$_B$.1-B*i***, **S2.2$_B$.2-B*i***, **S2.3$_A$.2-B11**, or **S4.2$_B$.1-B11** was suspended in 3 mL PBS (80 mM) containing 0.05% BSA and 50 ppm of the corresponding dye (Rh101 for **S2.2$_B$.1**, **S2.2$_B$.2**, or **S4.2$_B$.1-B11**, SRB for **S2.3$_A$.2-B11**). A total of 300 μL fractions of these suspensions (0.5 mg mL^{-1}) were then spiked with 3 μL of the corresponding serum **B*i*** (*i* = **4**, **5**, **8** or **11**) at a dilution of 1/100 (v/v). Again, the corresponding dye was added during the capping process to minimize dye release during incubation. Suspensions were stirred for 1 h at room temperature, centrifuged for 10 min at 9500 rpm and the resulting materials **S2.2$_B$.1-B*i*** (*i* = **4**, **5**, **8**), **S2.2$_B$.2-B*i*** (*i* = **4**, **8**, **11**), **S2.3$_A$.2-B11**, and **S4.2$_B$.1-B11** were washed following the same procedure described above for **S2.1$_E$.1-B5**. The materials were dried under vacuum overnight and stored at 4 °C. Materials prepared according to this procedure could be used for >6 months with unaltered performance, whereafter the amount of dye that could be maximally released decreased, and a certain blank release was also noticed.

*2.6.4. General Synthesis of the Antibody Capped Materials **S5.2$_B$.2-B11, S5.3$_A$.2-B11, and S5.4$_B$.2-B11**.* These hybrid materials were obtained as described above, only that a dilution of serum of 1/200 instead of 1/100 was employed.

*2.6.5. Kinetic Release Experiments with **S2.1$_E$.1-B5**.* To study the response of **S2.1$_E$.1-B5** in the absence and the presence of the analyte TATP, two fractions of 50 μL of **S2.1$_E$.1-B5** in PBS prepared with dilutions of 1/400, 1/200, and 1/100 (0.09 mg mL^{-1}) were deposited in a microtiter plate, and 5 μL of Milli-Q water were added to one, 5 μL of water containing 50 ppm of TATP to the other fraction. The fluorescence of the dye released in the suspensions was recorded by measuring the emission of FLU centred at 535 nm upon excitation at 490 nm using a microplate reader.

2.6.6. General Procedure for Kinetic Release Experiments with Antibody-Capped Materials. Section S4, SI, describes in more detail the procedures according to which the different experiments were performed. In general, 150 or 200 μg of antibody-capped materials were resuspended in 0.5 mL of PBS and split into two fractions of 0.25 mL. Subsequently, 0.5 or 3.65 mL of PBS were added to both fractions, whereas 75 or 100 μL of Milli-Q water was added to one fraction and 75 or 100 μL of water containing a certain amount of TATP was added to the other fraction, resulting in concentrations of 0.025 or 0.09 mg mL^{-1} solid and 3.5, 4.5, 7, or 10 ppm of TATP. When the effect of MeOH was assessed, the corresponding amount was also added to arrive at a final concentration of 2.5% (v/v). The suspensions were stirred at room temperature for 20 min up to 3.5 h, collecting fractions of 100 μL at different times. These fractions were centrifuged (10 min at 9500 rpm) to remove the gAID materials, and 60 μL of the corresponding supernatants were transferred into a black quartz cell with an optically active volume of 3 × 15 × 3 mm. The fluorescence of the supernatants was recorded at 595 nm (λ_{ex} = 576 nm, Rh101), at 582 nm (λ_{ex} = 564 nm, SRB), and at 582 nm (λ_{ex} = 555 nm, RhB). Table S3 contains an overview of the various procedures.

2.6.7. General Procedure for TATP Detection Studies with Capped Materials. Section S5, SI, details the procedures for the response studies performed. In general, 150 μg of a capped material was suspended in 1.5 mL of PBS and split into fractions of 100 or 140 μL. Each fraction was either not diluted or diluted with 250 μL PBS before 10 or 50 μL of PBS solutions containing different amounts of TATP were added to each fraction. The suspensions were stirred for certain time intervals, and after centrifugation, the fluorescence of the supernatants was recorded as described above. Table S4 contains the main parameters modified during the assays.

*2.6.8. Selectivity Studies with **S2.2$_B$.1-B4** and **S2.2$_B$.1-B5** at a Concentration of 0.09 mg mL^{-1} of Material.* A total of 150 μg of **S2.2$_B$.1-B4** and **S2.2$_B$.1-B5** was suspended in 1.5 mL of PBS, split into fractions of 140 μL, and 10 μL of a 40 ppm solution (in PBS) of TNT, RDX, PETN, HMX, NG, HMTD, and the educts of TATP synthesis (hydrogen peroxide, acetone and 7-octanoic acid, abbreviated 7-oxo), as well as various structurally related substances but-TP, 3-pent-TP, 2-pent-TP, DADP, 18-crown-6, and 12-crown-4 were added; for chemical structures, see Figure S5, SI. The suspensions were stirred for 1 h before the fluorescence of the supernatants was recorded after centrifugation as described above.

*2.6.9. Selectivity Studies with **S2.2$_B$.1-B4**, **S2.3$_A$.2-B11**, and **S5.3$_A$.2-B11** at Concentrations of 0.025 mg mL^{-1} of Material.* The studies were performed as described above; only that in this case, the fractions of materials were additionally diluted with 250 μL PBS (in case of **S2.3$_A$.2-B11**) or 240 μL PBS and 10 μL MeOH (for **S2.2$_B$.1-B4** and **S5.3$_A$.2-B11**) before 50 μL of 160 ppm of the potential cross-reactants listed above were added. The suspensions were stirred for 2 min (**S2.2$_B$.1-B4** and **S2.3$_A$.2-B11**) or 5 min (**S5.3$_A$.2-B11**), and after centrifugation, the fluorescence of the supernatants was recorded as described above for dyes Rh101 and SRB.

2.7. Lateral Flow Assays. *2.7.1. Lateral Flow Assays (LFAs) with Strips of 4 cm Length.* Nitrocellulose strips of 0.5 × 4 cm were manually cut with a cutter machine, and 1 μL of suspensions (2 mg mL^{-1}) of the gAID materials **S2.3$_A$.2-B11** and **S5.3$_A$.2-B11** were deposited in zone A with a micropipette, at ca. 1 cm from the bottom of the strip (see, e.g., Figure S16, SI). The strips were then dipped into 100 μL of buffered solutions containing various amounts of TATP. After 90 s of development, the test strips were dried using a hairdryer (in cold air blow mode for 15−30 s), to obtain a stable fluorescence signal (residual liquid on the strip influences the fluorescence of the dye), and the fluorescence was measured with a flow assay reader at 625 nm (λ_{exc} = 520 nm). If measurements were to be carried out after drying at room temperature under a normal atmosphere, 8 min are necessary to achieve a stable fluorescence.

2.7.2. LFAs with Strips of 2.5 cm Length. The procedure of preparation was the same as described above only that strips of 0.5 × 2.5 cm were cut and 0.5 μL of suspensions (2 mg mL^{-1}) of the gAID materials **S2.3$_A$.2-B11** and **S5.3$_A$.2-B11** were deposited in zone A with a micropipette, at ca. 0.2 cm from the bottom of the strip (see Figure S16, SI). TATP detection was performed according to the procedure in the preceding paragraph.

2.7.3. Strips Prepared with an Automatic Dispenser. The procedure of preparation was again similar, only that 50 nL of suspensions (2, 5, or 10 mg mL^{-1}) of **S2.3$_A$.2-B11** were deposited in zone A of strips of 0.5 × 2.5 cm with a sub-microliter piezoelectric dispenser, at ca. 0.2 cm from the bottom of the strip. TATP detection was performed following the same procedure as described above.

https://doi.org/10.1021/acsanm.1c03417
ACS Appl. Nano Mater. 2022, 5, 626−641

Scheme 1. Schematic Representation of the Architecture of (a) the Singly Silane-Functionalized gAID Materials S2.X_Y.Z and (b) of the Doubly Silane-Functionalized gAID Materials S4.2_B.1 and S5.X_Y.2 (X: cargo FLU = 1, Rh101 = 2, SRB = 3; Y: cargo loading medium EtOH = E, ACN = A, PBS = B; Z = hapten derivative, explanation see text and Table 1) and Their Analyte-Triggered Uncapping and Release Mechanism, the Chemical Structure of the Haptens I and II, the Hapten Silane Derivatives III and IV, the Non-Reactive Group, and the Antigen Triacetone Triperoxide (TATP)

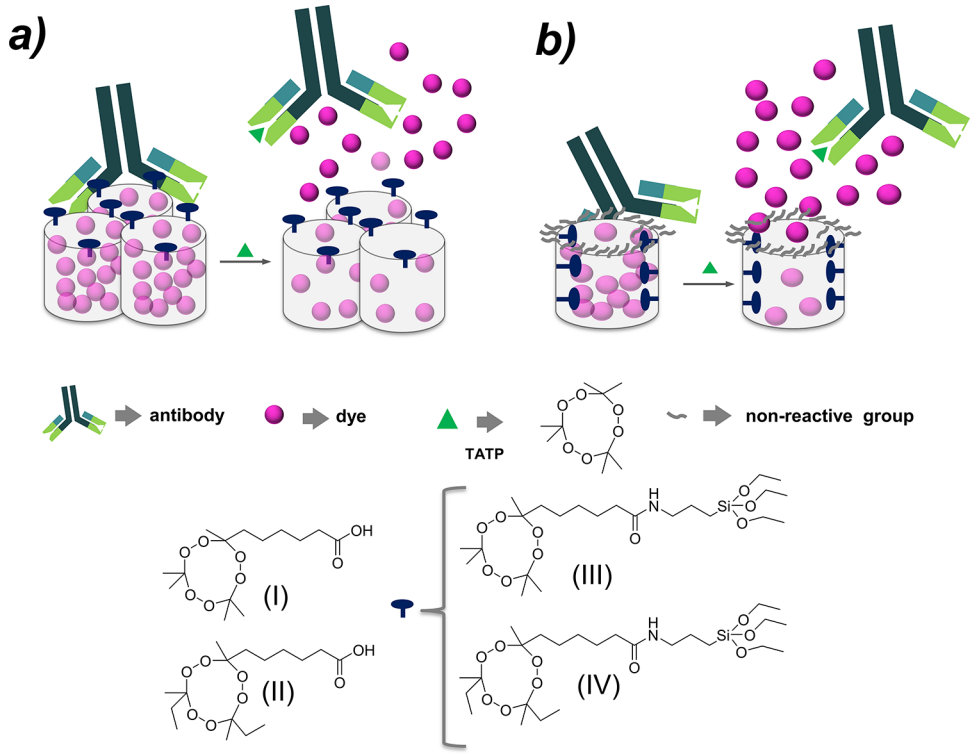

3. RESULTS AND DISCUSSION

3.1. Design of Gated Materials. A schematic representation of the system architecture and sensing paradigm is depicted in Scheme 1a. To study the closing/opening protocol of the gated ensemble, indicator dyes were first loaded into the mesopores of the silica particles. Then, the external surface of the particles was functionalized with a hapten silane derivative. Finally, the mesopores were capped with antibodies contained in the selected rabbit serum, hindering the dyes from escaping. As illustrated in Scheme 1a, in the analytical reaction, the corresponding antigen (complementary to the antibody) present in a sample is able to induce the uncapping of the pores and release of the entrapped guest. Thus, the state of the gated system can be easily monitored via the fluorescence of the dye released, i.e., for instance, in the supernatant after centrifugation of the mesoporous silica particles.

The key step of the development of immunogens for small molecules is the preparation of suitable haptens.[52−54] A hapten should preserve, as much as possible, the chemical structure, electronic distribution, and spatial conformation of the target analyte while introducing an appropriate linker to allow covalent attachment to the carrier. On the other hand, an important feature when aiming to use a capped hybrid delivery system is to obtain a highly selective and sensitive response while guaranteeing fast response times. Considering that highly selective and sensitive immunological responses are best obtained with high-affinity antibodies, which, however, could possess rather slow dissociation constants with the haptens, we decided to compare the effect of the hapten selected on the kinetic rates. For that purpose, two different haptens were prepared and evaluated. First, we used the same hapten as for the immunization, in particular, its silane derivative **III**, yielding materials **S2.1$_E$.1** and **S2.2$_B$.1** (for nomenclature of materials, see Table 1). For these materials, an analytical assay would result in the competition of TATP with its direct conjugate analogue, presumably entailing a rather slow response because the antibody shows a higher affinity for the hapten.[40] For the second series of gAID materials, we used a slightly mismatching hapten **II** (heterologous hapten[55−59]) and the corresponding hapten derivative **IV**. Because of the structural mismatch, lower affinities of the antibody for **IV** can be expected, potentially favoring competition by the target analyte. To test **IV**, the external surface of the silica particles was functionalized with this silane, leading to **S2.2$_B$.2** and **S2.3$_A$.2**. The choice of SRB instead of FLU was based on our recent studies of the loading/delivery behavior of dyes into/from mesoporous silica particles.[36]

Another factor that is expected to have an influence on such type of sensory system is related to the amount of hapten derivative anchored to the external surface of the mesoporous silica particles. If the degree of surface functionalization with haptens close to the pore outlets is (too) high, hapten crowding might happen at the surface, preventing efficient binding of antibodies, and many available haptens might lead to bivalent binding of the antibody, which slows down response times. We thus prepared **S4.2$_B$.1**, for which the external surface is blocked by a non-reactive group (propyl silane), and hapten derivatives are only anchored to the inner pore walls, allowing the binding of antibodies to hapten preferentially at the upper rim of the pore outlets.[29] This

https://doi.org/10.1021/acsanm.1c03417
ACS Appl. Nano Mater. 2022, 5, 626−641

Table 1. Composition of the 17 Materials Prepared in this Work, Sn.X_Y.Z with n = 1−5 (Type of Material), X = 0−4 (Cargo), Y = A, B, E (Loading Medium), Z = 1, 2 (Hapten Derivative)

material[a]	silica scaffold[b]	dye[c]	solv.[d]	passiv.[e]	H.[f]
S1	MCM-41$_{as}$	–	–	–	–
S2	MCM-41	–	–	–	–
S3	SBA-15$_{as}$	–	–	–	–
S4	**S1**	–	–	+	–
S5	**S3**	–	–	+	–
S2.1$_E$.1	**S2**	FLU	EtOH	–	**III**
S2.2$_B$.1	**S2**	Rh101	PBS	–	**III**
S2.2$_B$.2	**S2**	Rh101	PBS	–	**IV**
S2.3$_A$.2	**S2**	SRB	ACN	–	**IV**
S4.0.1	**S4**	–	–	+	**III**
S4.2$_B$.1	**S4**	Rh101	PBS	+	**III**
S5.0.2	**S5**	–	–	+	**IV**
S5.2$_A$.2	**S5**	Rh101	ACN	+	**IV**
S5.2$_B$.2	**S5**	Rh101	PBS	+	**IV**
S5.4$_A$.2	**S5**	RhB	ACN	+	**IV**
S5.4$_B$.2	**S5**	RhB	PBS	+	**IV**
S5.3$_A$.2	**S5**	SRB	ACN	+	**IV**

[a]Precursor materials **S1**−**S5**, sensory materials **Sn.X$_Y$.Z**. [b]Subscript "as" denotes as prepared mesoporous silica particles. [c]Dye used as cargo, FLU = 1, Rh101 = 2, SRB = 3, RhB = 4; no cargo = 0 in functionalized materials. [d]Solvent used for dye loading, EtOH = E, ACN = A, PBS = B. [e]Passivation of the external surface with propyltrimethoxysilane. [f]Hapten silane derivative, **III** = 1, **IV** = 2.

should not only improve dedicated interaction but is also more economical because the usage of an excess of antibody can be avoided.

To investigate the influence of the pore size, we prepared a series of SBA-15-type materials. These materials all contain an external propyl silane coating and the haptens **III** or **IV** attached to the inner pore walls. Especially for larger pore diameters, this localized two-step silane functionalization is expected to yield better pore closure because the antibody can only interact with the haptens anchored at the entrance region of the pores. Scheme 1b illustrates this design principle.

The suitability of the two different approaches for final TATP detection performance was investigated with 12 different materials, using different inorganic scaffolds (MCM-41 or SBA-15), hapten derivatives (**III** and **IV**), indicator dyes as cargo, and also non-reactive (passivating) groups. Material syntheses were accomplished as follows.

3.2. Synthesis and Characterization of Gated Materials. The precursor materials **S1**−**S3** were synthesized according to standard protocols reported by us previously,[21,51] employing surfactant templating. Primary and secondary silane functionalization of the as-prepared and calcinated silicas was also adopted from previous reports by others and us, following established silane coupling chemistry.[29,60] All materials were characterized with standard methods as described in detail in the SI, revealing particle diameters of 100 ± 20 nm as well as dimensions of 870 ± 80 × 480 ± 40 nm, pore sizes of 2.6 and 8.4 nm, and specific surface areas of 1053 $m^2\ g^{-1}$ and 860 $m^2\ g^{-1}$ for the MCM-41- and SBA-15-type scaffold materials, respectively. After loading and functionalization, the particle sizes were virtually unaltered, while the specific surface areas were distinctly reduced, e.g., to 263 $m^2\ g^{-1}$ for **S2.3$_A$.2**.

3.3. Optimization of the Amount of Capping Antibody. One of the key features of analyte-triggered release is the avoidance of dye leaching in the absence of an analyte. Such unintended signals would compromise performance and reproducibility, potentially generating false positives. It is thus essential to find the optimum amount of antibody that is necessary to block the pores efficiently. We selected material **S2.1$_E$.1** for these experiments because a dianionic dye such as fluorescein is known to be delivered rapidly from porous silica particles.[36] Preliminary studies were carried out with the serum collected after boost injection number 5 (**B5**). Aiming at immunochemical optimization, other sera obtained from boosts 4, 8, and 11 (**B4**, **B8**, and **B11**) were also tested under these conditions. The different studies that have been carried out are detailed below.

To find the optimum conditions for studying the interaction between the hapten anchored onto the surface of **S2.1$_E$.1** and the polyclonal TATP antibodies of **B5**, the influence of the medium on leaching of the dye from uncapped material was first assessed. Based on our previous studies,[29] portions of 150 μg of **S2.1$_E$.1** were suspended in 300 μL of two different buffers (PBS and PBS containing 0.05% BSA) by stirring for 1 h at room temperature. Afterward, the suspensions were centrifuged, and the amount of FLU released into the supernatant was monitored spectrophotometrically at 490 nm. Figure S6a shows that the addition of 0.05% BSA can significantly reduce native leaching (in absence of BSA and **B5**) to ca. 60% of dye within 1 h. Presumably, the presence of BSA helps to non-specifically block the pores in the absence of dedicated capping moieties. The incubation experiments were then repeated in the presence of serum **B5** at 1/100 dilution, showing that for both media, capping was already rather effective, reducing the amount of dye released to <40% within 1 h and <50% within 1 h in the presence and absence of BSA (Figure S6a).

Because a better efficiency of the capping was achieved in the presence of BSA, further experiments were carried out in PBS containing 0.05% of BSA. Furthermore, to minimize the amount of dye released during the capping process, FLU was added at 200 ppm to the PBS/BSA buffer. The presence of such a concentration of FLU in the medium in which the capping is carried out should partially inhibit the unintended release of dye from uncapped pores.

Next, the amount of antibody necessary for a complete capping of the pores of **S2.1$_E$.1** was determined, employing serum **B5** in different dilutions (1/1000, 1/500, 1/400, 1/200, 1/100) and the washing protocol detailed in the Experimental Section, Section 2.6.2. The results shown in Figure S6b indicate that an effective capping was only observed when the 1/100 or 1/200 dilutions of the serum of boost **B5** were used, with the 1/100 dilution (20% dye released after 30 min) outperforming the 1/200 dilution. With less antibodies, capping was less effective.

3.3.1. Delivery Studies in Presence of TATP. To study the response of **S2.1$_E$.1-B5** in the presence of the analyte TATP, the same experiment was repeated after spiking the buffer with TATP. A total of 50 μL of each suspension of **S2.1$_E$.1-B5** prepared with **B5** in dilutions of 1/100 and 1/200 was mixed with 200 μL of PBS containing 5 ppm of TATP. The release kinetics were again traced by registering FLU emission over time, allowing us to judge how far TATP competes favorably with the anchored hapten for the antibody's binding sites (Figure S7, SI). In the presence of TATP, the dye release was

https://doi.org/10.1021/acsanm.1c03417
ACS Appl. Nano Mater. 2022, 5, 626−641

similar for both **B5** dilutions. However, as dilution 1/100 showed less blank release, it yielded overall better results. Nonetheless, the data in Figure S7a also suggest that system performance should still be generally improvable, yet most likely not with FLU as the indicator cargo as a recent study of us has suggested.[36] Indeed, any further attempts to improve the performance of **S2.1$_E$.1-B5** were unsuccessful, presumably due to the low amount of FLU that can be loaded into the pores of MCM-41-type silica. We thus incorporated rhodamine 101 (Rh101) instead of FLU and prepared material **S2.2$_B$.1**.

Following the same procedure, we tested **S2.2$_B$.1** with the optimum conditions found for solid **S2.1$_E$.1**. As can be seen in Figure 2a, squares, and Figure S8, a behavior qualitatively

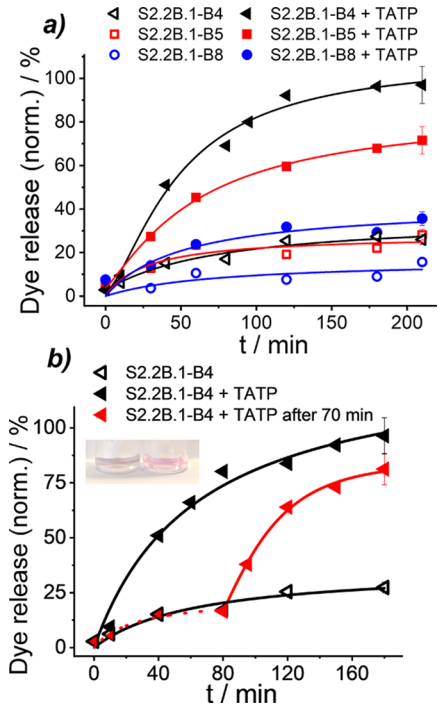

Figure 2. (a) Rh101 release over time from **S2.2$_B$.1** capped with sera **B4**, **B5**, or **B8**, i.e., from **S2.2$_B$.1-B4** (triangles), **S2.2$_B$.1-B5** (squares), and **S2.2$_B$.1-B8** (circles) at a concentration of 0.09 mg mL^{-1} in the absence (open symbols) and presence (solid symbols) of 4.5 ppm of TATP in PBS (pH 7.4). (b) Rh101 release from **S2.2$_B$.1-B4** over time in the presence (solid black triangle) and absence (open black triangle) of 4.5 ppm of TATP in PBS (pH 7.4). The red curve with triangles shows the release profile of Rh101 from **S2.2$_B$.1-B4** in PBS (pH 7.4) before and after the analyte is added at t = 70 min (final TATP concentration of 4.5 ppm). Inset: photograph showing dye release after 2 h in the absence (left) and presence (right) of TATP (9 ppm). In (a) and (b), the release was determined fluorometrically at 595 nm upon excitation at 576 nm. The lines are included only as a guide to the eye for better illustration.

similar to **S2.1$_E$.1-B5** was observed for **S2.2$_B$.1-B5**, yet the active release was higher. However, despite the latter, the response kinetics were slower. For a better comparison, for every material prepared, the amount of dye released in the different experiments was normalized to the maximum amount of dye that the respective material was able to release in the presence of an excess of TATP after full equilibration, i.e., after reaching a plateau in the kinetic release experiments; this amount of dye was set as 100% release.

3.3.2. Delivery Studies with Different Sera. Before addressing response kinetics, the influence of the affinity of the antibodies generated along the immunization period on the magnitude of dye delivery was assessed, carrying out analogous assays with sera of boosts **B8** and **B4** and material **S2.2$_B$.1**. Figure 2 compares the kinetics of the previous material **S2.2$_B$.1-B5** with **S2.2$_B$.1-B8** and **S2.2$_B$.1-B4** in the presence and the absence of 4.5 ppm of TATP in PBS at pH 7.4. It is obvious that most dyes can be released from **S2.2$_B$.1-B4** and least from **S2.2$_B$.1-B8**, which correlates well with the affinity constants of the antibodies of the different sera, increasing on the order of **B4** < **B5** < **B8** (Table S2). As would be expected, antibodies of **B4** are more easily displaced from the anchored hapten upon TATP addition than those of the other two sera.

*3.3.3. Selectivity and Cross-Reactivity Studies of **S2.2$_B$.1-B4** and **S2.2$_B$.1-B5**.* To get a first idea of the sensitivity of the system, the delivery of Rh101 from **S2.2$_B$.1-B4** was measured as a function of the concentration of TATP. The inset in Figure 3a shows that a clear dose−response behavior is found,

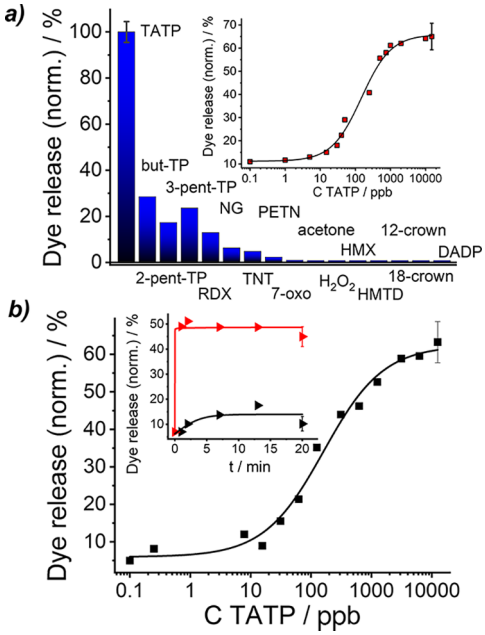

Figure 3. (a) Rh101 release from **S2.2$_B$.1-B5** (0.09 mg mL^{-1}) in the presence of 1 ppm of TATP or potentially cross-reacting compounds in PBS (pH 7.4) after 2.5 h incubation. Inset: Rh101 release from **S2.2$_B$.1-B4** (0.09 mg mL^{-1}) as a function of the concentration of TATP in PBS (pH 7.4) after 1 h of incubation. (b) Rh101 release from **S2.2$_B$.1-B4** as a function of the concentration of TATP in PBS containing 2.5% of MeOH (pH 7.4) after 2 min of incubation. The release was determined fluorometrically at 595 nm upon excitation at 576 nm. The line exemplifies a four-parametric logistic fit. Inset: Rh101 release from **S2.2$_B$.1-B4** (0.025 mg mL^{-1}) over time in the presence (red) and the absence (black) of 3.5 ppm of TATP in PBS containing 2.5% of MeOH as organic co-solvent (pH 7.4). The lines are included only as a guide to the eye for better illustration.

arriving at a limit of detection (LOD) of 15.2 ± 4.6 ppb of TATP. Moreover, an initial selectivity assessment was carried out for **S2.2$_B$.1-B4** and **S2.2$_B$.1-B5**. These materials were chosen because the difference between blank and analyte-triggered release was basically acceptable in analytical terms (Figure 2). As potentially cross-reactive species, some of the most common explosives such as TNT, RDX, PETN, HMX, NG, and HMTD were examined. Furthermore, the educts of

https://doi.org/10.1021/acsanm.1c03417
ACS Appl. Nano Mater. 2022, 5, 626−641

TATP synthesis (hydrogen peroxide, acetone, and 7-oxo) as well as various structurally related substances (but-TP, 3-pent-TP, 2-pent-TP, DADP, 18-crown-6, 12-crown-4; for chemical structures, see Figure S5, SI) were prepared and their potential cross-reactivities were assessed. The uncapping ability of these molecules (at 1 ppm concentration) is shown in Figure 3a and Figure S9a, SI. A promising selectivity for TATP was found for both materials, with **S2.2$_B$.1-B5** exhibiting a better suppression of cross-reactivity toward non-peroxidic compounds, which is presumably due to longer affinity maturation.

The direct interference by competition of the potentially cross-reacting compounds was addressed in another assay by suspending **S2.2$_B$.1-B4** and **S2.2$_B$.1-B5** in solutions containing equimolar amounts (1 ppm) of TATP and the respective compounds. In the case of **S2.2$_B$.1-B5**, a similar dye release within the experimental error was observed for TATP alone and for the mixtures (Figure S9b, SI). In contrast, for **S2.2$_B$.1-B4**, various potentially competing compounds showed a higher release than 1 ppm TATP, indicating that selectivity is better for **S2.2$_B$.1-B5**.

3.3.4. Optimization of Response Time. The results obtained so far led to the conclusion that if Rh101 is used as indicator dye in combination with the capping approach shown in Scheme 1a, i.e., coating the outer surface of the mesoporous particles with the hapten derivative, the hybrid ensemble performs already rather selective and sensitive with respect to TATP detection. Some interference is found for other peroxide-based explosives (PBEs), yet the selectivity against other explosives and especially H_2O_2 is very good. The detection limit of 15.2 ± 4.6 ppb of TATP is also acceptable for a simple system such as the present one. Unfavorable, however, are the long equilibration times that are necessary to achieve significant release resulting in pronounced signals (ca. 70%), i.e., 1 h in the case of **S2.2$_B$.1-B4** and even 2.5 h in the case of **S2.2$_B$.1-B5**.

To improve these features, several optimization steps were carried out for **S2.2$_B$.1-B4**. First, conditioning and storage of the materials after capping and removal of dye from uncapped pores by washing were optimized, revealing that vacuum-drying overnight and storage at 4 °C did not only retain performance but also allowed to use the material for >6 months with unaltered performance. Second, the amount of material used in an assay was optimized, yielding the best improvement in terms of release kinetics for a concentration of 0.025 mg mL^{-1} of **S2.2$_B$.1-B4**, which allowed to achieve delivery of 75% of the dye after ca. 20 min instead of 1 h (cf. Figure S10, SI and Figure 2). While these conditions led to a significant acceleration, the LOD for TATP was slightly higher, 26.9 ± 11.3 ppb (Figure S10, SI).

The main reason for the slow response to TATP is most likely that the TATP antibody binds approximately fourfold stronger to hapten **I**, used for animal immunization, than to neat TATP.[40] This high affinity may cause slow off-rates, which are detrimental in this format. Thus, tuning of the binding strength between antibody and immobilized hapten should be the key factor for an acceleration of dye release. One possibility to achieve this is the use of organic co-solvents. Obviously, as the structure of the antibody should remain intact, the use of an organic co-solvent is limited.[61−63] Release experiments were thus performed after adding different amounts of MeOH and DMSO (between 1−10%) to suspensions of **S2.2$_B$.1-B4** in PBS. Tolerance of the antibody of up to 2.5% MeOH was found, whereas the system did not tolerate DMSO even at 1%, which led to a fast release of dye in the absence of TATP. However, with the addition of 2.5% of MeOH, a quasi-instantaneous displacement of the dye was only observed in the presence of TATP, improving the response time dramatically (Figure 3b). Using these conditions, i.e., suspensions of 0.025 mg mL^{-1} of **S2.2$_B$.1-B4** in PBS containing 2.5% of MeOH, dye delivery as a function of the concentration of TATP was always fast and completed in only 1−2 min while yielding an LOD of 11.2 ± 2.3 ppb (Figure 3b). Table 2 summarizes the major optimization steps.

Table 2. Major Optimization Steps for S2.2$_B$.1-B4 Including the Concentration of Material ($c_{S2.2B.1-B4}$) and the Amount of Co-Solvent MeOH (V_{MeOH}); t_r = Response Time, WR_{TATP} = Working Range and LOD_{TATP} = Limit of Detection for TATP

step	$c_{S2.2B.1-B4}$/ mg mL^{-1}	V_{MeOH}/%	t_r/min	WR_{TATP}/ ppb	LOD_{TATP}/ ppb
1	0.09		60	30−1000	15.2 ± 4.6
2	0.025		20	35−10,000	26.9 ± 11.3
3	0.025	2.5	1−2	32−1000	11.2 ± 2.3

These results show that parameters such as the amount of material used, or the presence of an organic co-solvent can significantly reduce response times from ca. 1 h to a few minutes. However, as the presence of organic auxiliary agents seems to be critical for the TATP antibody, another strategy was invoked, namely, hapten heterology.[55−59] This approach relies on the employment of slightly mismatched hapten derivatives and strongly binding antibodies like clones obtained from late immunization boosts during antibody production. This approach accelerates particularly off rates, potentially making short assay times possible, and is especially relevant in the case of bivalent antibody binding.[57] The relative binding strength of peroxide analogues but-TP, 3-pent-TP, 2-pent-TP, and DADP were thus compared to that of hapten derivative **III**, singling out but-TP as the most potent candidate. In the next optimization step, hapten derivative **III** was thus exchanged for **IV**.

3.4. Exchange of Hapten Derivative III by IV. First, comparative studies with the currently preferred serum of boost 4 (**B4**) and hapten derivative **IV** were carried out. It is expected that **IV** has less affinity for the antibodies than **III**, showing faster release kinetics. For this purpose, materials **S2.2$_B$.2** and **S2.3$_A$.2** were prepared, incorporating Rh101 loaded in PBS buffer (**S.2.2$_B$.2**) and SRB loaded in ACN (**S2.3$_A$.2**) while expressing hapten derivative **IV** as the gatekeeper in the ensemble. Then, the performance of stronger binding antibodies from sera **B8** and **B11** was assessed.

3.4.1. Capping and Delivery Studies with Hapten Derivative IV. Material capping and kinetic release experiments with **S2.2$_B$.2-B*i*** with ***i*** = **4**, **8**, and **11** were carried out as described in the Experimental Section, Section 2.6.7 and section S4.2, SI, in analogy to those involving **S2.2$_B$.1-B4**. Figure 4a shows the kinetic release of **S2.2$_B$.2-B11** in the presence and the absence of 7.5 ppm of TATP. As can be seen, the release of the dye in the presence of TATP is virtually instantaneous, despite the use of a strongly binding clone. This beneficial behavior is presumably related to the rationale outlined above, the acceleration of dissociation rates between heterologous hapten and high-affinity antibody.

https://doi.org/10.1021/acsanm.1c03417
ACS Appl. Nano Mater. 2022, 5, 626−641

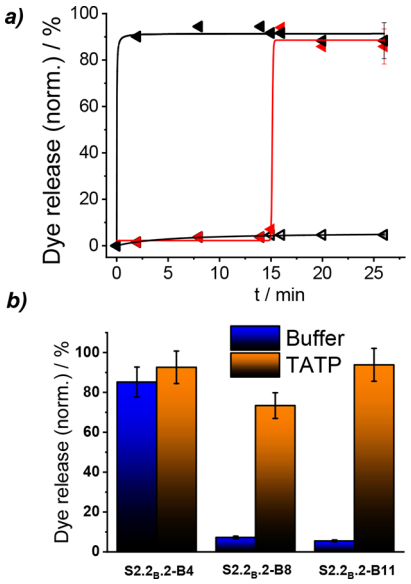

Figure 4. (a) Rh101 release from **S2.2$_B$.2-B11** (0.025 mg mL^{-1}) over time in the presence (solid black triangles) and the absence (open triangles) of 7.5 ppm of TATP in PBS (pH 7.4). The red curve with triangles shows the release profile of Rh101 from **S2.2$_B$.2-B11** in PBS (pH 7.4) before and after the analyte is added at t = 70 min (final TATP concentration of 7.5 ppm). The release was determined fluorometrically at 595 nm upon excitation at 576 nm. The lines are included only as a guide to the eye for better illustration. (b) Relative Rh101 release from **S2.2$_B$.2-B4**, **S2.2$_B$.2-B8** and **S2.2$_B$.2-B11** (0.025 mg mL^{-1}) in the presence (orange) and the absence (blue) of 7.5 ppm of TATP in PBS (pH 7.4) after 2 min. Release was determined fluorometrically at 595 nm upon excitation at 576 nm.

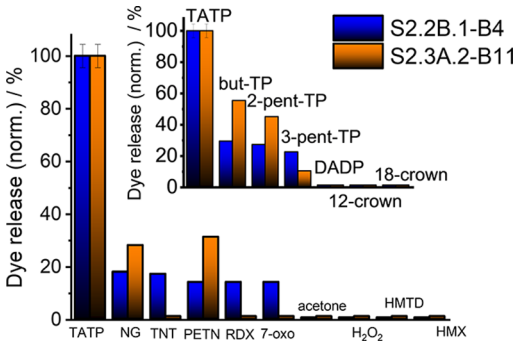

Figure 5. Relative SRB (orange bars, **S2.3$_A$.2-B11**) and Rh101 (blue bars, **S2.2$_B$.1-B4**) release in the presence of TATP or potentially cross-reacting compounds (2 ppm) in PBS (**S2.3$_A$.2-B11**, pH 7.4) or PBS containing 2.5% MeOH (**S2.2$_B$.1-B4**) after 2 min of incubation (for 0.025 mg mL^{-1} material). Release was determined fluorometrically at 582 nm (595 nm) upon excitation at 564 nm (576 nm).

S2.2$_B$.2-B8 offers a similar response, but in this case, the amount of dye released was lower. In contrast, **S2.2$_B$.2-B4** was not able to discriminate between the presence and the absence of TATP, showing massive blank release (Figure 4b). The latter is ascribed to the combination of a weakly binding antibody (**B4**) and a heterologous hapten **IV**, being unable to close the pores efficiently because of a very low overall binding constant. On the other hand, the small difference between **B8** and **B11** can be ascribed to the small difference in the affinity constant values of each serum, **B11** being only 1.5-fold more affine to TATP than **B8** (Table S2).

S2.3$_A$.2-B11 showed a similar kinetic behavior as **S2.2$_B$.2-B11**. However, because SRB allows for more sensitive detection, the LOD of 19.6 ± 4.3 ppb for **S2.2$_B$.2-B11** could be lowered to 12.5 ± 2.1 ppb (for 2 min incubation time, see Figure S11, SI).

*3.4.2. Selectivity and Cross-Reactivity of **S2.3$_A$.2-B11**.* Following the same procedure as in the case of the materials being functionalized with hapten derivative **III**, dye delivery from **S2.3$_A$.2-B11** was assessed for potentially interfering compounds. The results are collected in Figure 5. Apparently, the cross-reactivity of **S2.3$_A$.2-B11** toward closely related cyclic peroxides and the acyclic explosives NG and PETN is higher than that of **S2.2$_B$.1-B4**, the best performing material using **III**, yet an improvement in selectivity was found against the other aromatic and cyclic nitro-containing explosives. Overall, the performance with respect to potential interference by application-relevant species was better for **S2.3$_A$.2-B11**.

3.5. Positioning of Hapten Derivative. Being aware of the influence of the positioning of the hapten derivative on the inner and/or outer surface of the host particle on the performance of gAID systems,[29] as-synthesized MCM-41 **S1** was first passivated on the outer surface with short yet non-interacting propyl groups (**S4**) before hapten derivative **III** was grafted to the inner pore walls, resulting in **S4.2$_B$.1**, and compared to the corresponding material **S2.2$_B$.1** (Scheme 1b). Because the accessibility of the hapten is aggravated by moving it deeper into the pore openings, the stronger binding hapten **III** was used here. However, for **S4.2$_B$.1**, only negligible differences were observed in the absence and the presence of TATP, suggesting that a location of the hapten molecules only at the inner pore walls prevents already a strong interaction with a capping antibody, presumably because the mesopores of MCM-41 are rather narrow. Exchange of the MCM-41-type by an SBA-15-type scaffold promises to lead to an improvement here,[29] SBA-15 possessing larger pore sizes of >8 nm.[64,65] Wider pores would help to increase the mobility of the antibody inside of the pore openings, facilitating correct spatial orientation for optimal interaction with the hapten. A series of SBA-15 analogues to **S4.2$_B$.1** were thus prepared.

3.5.1. Choice of Optimal Dye and Loading Conditions for S5 Materials. The delivery capacities of materials **S5.2$_A$.2**, **S5.2$_B$.2**, **S5.3$_A$.2**, **S5.4$_A$.2**, and **S5.4$_B$.2** were studied by suspending 1 mg of each solid in 1 mL of PBS (pH 7.4) and stirring for 2 min. After centrifugation, the dye released was quantified via absorption measurements at their respective absorption maxima (Figure S12, SI). Large differences as a function of dye and loading medium were found, with **S5.3$_A$.2** showing the most efficient delivery of its SRB cargo. Materials **S5.2$_B$.2** and **S5.4$_B$.2** showed the next best performance while loading of Rh101 and RhB in ACN did only lead to very poor delivery from **S5.2$_A$.2** and **S5.4$_A$.2**. These results are in line with our previous work on loading and release studies.[36]

*3.5.2. Capping and Delivery Studies with **S5.2$_B$.2**, **S5.3$_A$.2** and **S5.4$_B$.2**.* With promising larger-pore materials at hand, the next step involved the capping and performance testing of the SBA-15 materials containing hapten derivative **IV** anchored to the inner walls, thus being able to interact with antibodies only directly at the rim of the pore openings. The materials were capped according to the same procedure as described above for the MCM-41 materials by preparing solutions of **B11** in PBS containing 0.05% BSA and 150 ppm of Rh101 (for **S5.2$_B$.2**), RhB (for **S5.4$_B$.2**), and SRB (for **S5.3$_A$.2**) while using different serum dilutions (1/1000, 1/500, 1/400 and 1/200 at pH 7.4).

https://doi.org/10.1021/acsanm.1c03417
ACS Appl. Nano Mater. 2022, 5, 626−641

After each solution was stirred for 1 h at room temperature, portions of 150 μg of **S5.2$_B$.2**, **S5.3$_A$.2**, and **S5.4$_B$.2** were suspended in 300 μL of the serum-containing solutions and stirring was continued for 1 h at room temperature. The resulting materials were washed five times with 300 μL with PBS, centrifuged, and stored at 4 °C, yielding **S5.2$_B$.2-B11**, **S5.3$_A$.2-B11**, and **S5.4$_B$.2-B11**.

The kinetic release behavior was then assessed for **S5.2$_B$.2-B11**, **S5.3$_A$.2-B11**, and **S5.4$_B$.2-B11** in a similar way as outlined previously. Working with this protocol, no difference in the release behavior in the presence and the absence of TATP was observed for serum dilutions lower than 1/400. In all the cases, dye release increased with time, i.e., blank delivery dominated. Among all materials, **S5.3$_A$.2-B11** offered the best performance, showing a noticeable release of dye after ca. 5 min (with serum dilution of 1/200) and 10 min (with 1/400 dilution; Figure S13a,b, SI). Materials **S5.2$_B$.2-B11** and **S5.4$_B$.2-B11** showed slower release kinetics, with a noticeable release of dye in the presence of TATP only after 30 min (Figure S13c,d, SI).

Based on the previous results obtained for the MCM-41-type gAID materials, and with the aim to reduce the response time, 2.5% of MeOH was added as co-solvent. For all the three cases **S5.2$_B$.2-B11**, **S5.3$_A$.2-B11**, and **S5.4$_B$.2-B11**, uncapping was now favorably fast (Figure S14, SI). A comparison of the data reveals that whereas 80% of dye was released in <5 min from **S5.3$_A$.2-B11**, 10−15 min were required to reach almost quantitative delivery from **S5.2$_B$.2-B11** and **S5.4$_B$.2-B11**, stressing the superior performance of SRB. The sensitivity against TATP was also studied as described above, i.e., in suspensions of 0.025 mg mL^{-1} material in PBS containing 2.5% of MeOH while using incubation times of 5 min for **S5.3$_A$.2-B11** and 20 min for **S5.2$_B$.2-B11** and **S5.4$_B$.2-B11**. The best performance was found for **S5.3$_A$.2-B11** with a limit of detection of 19.4 ± 5.6 ppb.

*3.5.3. Selectivity and Cross-Reactivity of **S5.3$_A$.2-B11**.* Following the same procedure used previously for the MCM-41-type materials containing hapten derivative **IV**, dye delivery from **S5.3$_A$.2-B11** was tested against potentially cross-reacting species. Figure S15 collects these results and reveals that despite employing boosts with high-affinity clones, this strategy in which the hapten is located only on the inner walls of the mesopores offers less selectivity in comparison with the system in which the hapten is grafted to the outer surface.

3.6. Amplification Features of gAID Systems. Because gAID systems are able to release a much larger number of indicator molecules in the presence of considerably few analyte molecules, we estimated the amplification factors of the materials and chose an analyte concentration that produces a dye release equivalent to 15% of the maximum signal as the reference point. Immanent in the design of such systems is the fact that chemical amplification depends on concentration, i.e., the amplification factor decreases with an increase in analyte concentration. As can be seen in Table S5, for instance, **S2.2$_B$.1-B4** carrying hapten derivative **III** and Rh101 was able to release more dye in comparison with its analogue **S2.2$_B$.2-B11**. Furthermore, SRB was easily released from the MCM-41 scaffold of **S.2.3$_A$.2-B11**, showing the best amplification factor while containing hapten derivative **IV**.

3.7. Lateral Flow Assays. After the system was optimized in suspension assays, yielding LODs of 12 and 19 ppb as well as dynamic ranges of 30−1000 and 70−800 ppb at assay times of 2 and 5 min for the MCM-41-type and the SBA-15-type materials **S2.3$_A$.2-B11** and **S5.3$_A$.2-B11** and demonstrating the advantage of the combination of high-affinity antibodies and slightly mismatched, i.e., heterologous haptens, we proceeded to integrate the mesoporous gAID materials with a lateral flow assay (LFA) to assess whether the favorable performance parameters can be retained in such a uniquely simple assay format. Such assays commonly rely on test strips that carry the (bio)chemical part of the detection system and that after dipping the test strip into the sample solution and evolution of the flow, develop a color that can be perceived by the eye. These types of assays are rapid, sensitive, specific, cheap, and easy to handle, with clear advantages in routine applications by untrained personnel or in emergency cases. However, they require protein conjugates to travel the active distance of the strip, which renders them prone to errors due to unspecific binding. Considering these procedures, we designed a similar approach for the detection of TATP (Scheme 2). The strip

Scheme 2. Design and Principle of Operation of the Lateral-Flow Assay: (a) Si.3$_A$.2-B11 (*i* = 2, 5) Is Deposited at Zone A so that the Strip can be Conveniently Dipped into the Sample; (b) the Presence of the Analyte Leads to (Partial) Uncapping of the Pores and Release of the Dye, which is Transported at the Solvent Front; (c) after Development and Drying, Zone B Contains the Amount of Dye that Corresponds to the Amount of Analyte in Solution while Zone A Contains the Residual, Unreleased Dye in Still Capped Pores

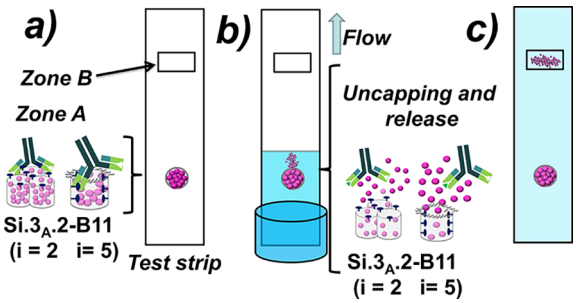

also contains an interaction and a detection zone. While the gAID material is located in the interaction zone A, where the response is generated, the detection zone B is an arbitrary area at the solvent front in which a signal is collected (Scheme 2c). The TATP detection protocol relies on the following approach: if a strip is introduced into a sample that does not contain the analyte (TATP), no dye release would be observed, and no signal would be detected in zone B. However, when TATP is present in the sample, a proportional number of pores of the gAID material would be uncapped because of TATP binding to the antibody, releasing their cargo, which can travel with the solvent front toward zone B while the particles do not travel with the flow and remain in zone A (Scheme 2b). The amount of TATP in the sample thus determines the amount of released dye and hence the fluorescence signal that can be detected in zone B.

In contrast to small gold nanoparticles used in conventional immunochemical LFAs such as pregnancy tests, the mesoporous silica particles used here are too large to be transported by an aqueous flow in the strip's membrane, so that dye cargo residing in still capped pores is retained at the spot of deposition (Scheme 2c and Figure 6a, zone A), allowing for an internal referencing of the signal measured in the detection

https://doi.org/10.1021/acsanm.1c03417
ACS Appl. Nano Mater. 2022, 5, 626−641

zone B and avoiding the use of a control line as in the pregnancy test.

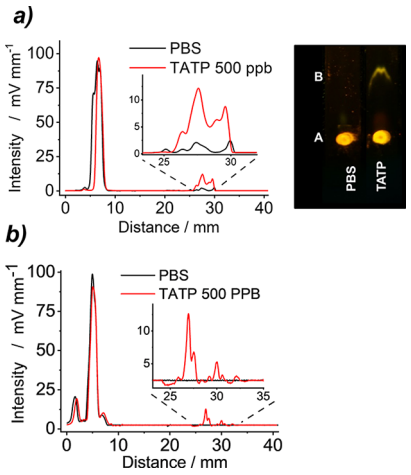

Figure 6. Signals obtained with a LFA reader (λ_{exc} = 520 nm, λ_{em} = 625 nm) in zones A and B after dye release from **S2.3$_A$.2-B11** (a) and **S5.3$_A$.2-B11** (b) and development of the flow in the absence (black lines) and the presence (red lines) of 0.5 ppm TATP in PBS buffer (pH 7.4). Zone A is at ca. 5−8 mm, and zone B is at ca. 26−30 mm. Insets show a magnification of the zones B. The image in (a) shows both strips under LED excitation when photographed with a smartphone setup,[30] using an LED of 490 nm as excitation source powered by the smartphone via a USB-OTG link and filtered by a short-pass filter (532 nm) while collecting the emission through a long-pass filter (550 nm) after inserting the developed strip in a 3D-printed, customized holder.

A high-flow nitrocellulose membrane was selected as the support for the LFA studies and turned into a test strip as described in the Experimental Section, Section 2.7. The assay workflow consists of dipping the strips into a buffered solution, 90 s of development, drying for 15−30 s, and measuring of the fluorescence with a flow assay reader. The fluorescence traces of two strips are depicted in Figure 6, obtained for **S2.3$_A$.2-B11** and **S5.3$_A$.2-B11** and a sample containing 0.5 ppm of TATP. Whereas control samples containing only PBS produced only a negligible fluorescence in zone B (Figure 6, black lines), a clear signal was found in zone B for the samples with TATP (Figure 6, red lines). Furthermore, when the strips were introduced into a case fit onto a smartphone as recently reported by us[30] and adequately excited, the fluorescence of zone A containing the spot of the material **S2.3$_A$.2-B11** was clearly observed on both strips, whereas a fluorescence signal in zone B was only visible in the presence of TATP, ascribed to the SRB released from the material (see Figure 6a).

Following the same procedure as in the suspension studies, the effect of the TATP concentration was studied for the LFA format. The amount of dye released for each concentration was calculated from the ratio of the area of zone B and the total area of the test strip. Figure 7 shows the dye release as a function of the amount of TATP, clearly exhibiting qualitatively similar behavior as in suspension though reaching slightly worse LODs of 50.3 ± 6.6 ppb for **S2.3$_A$.2-B11** and 62.3 ± 8.6 ppb for **S5.3$_A$.2-B11**. In the absence of TATP, no signal was found in zone B.

The effect of the educts of TATP synthesis, other explosives, and other peroxides was also assessed in cross-reactivity studies, and the results in terms of selectivity were similar to

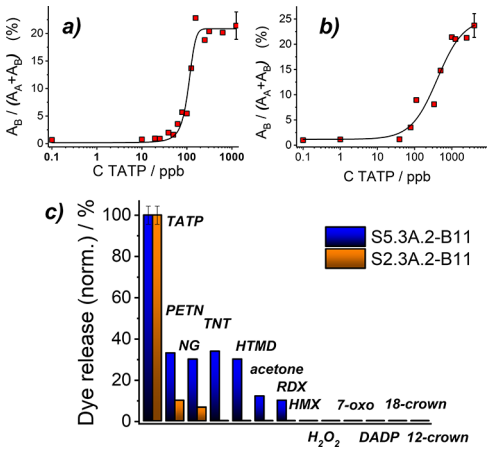

Figure 7. SRB release from **S2.3$_A$.2-B11** (a) and **S5.3$_A$.2-B11** (b) on test strips in zone B with respect to the total area of the strip (in %) as a function of TATP concentration. Release was determined fluorometrically at 620 nm upon excitation at 520 nm with an LFA reader. The lines exemplify four-parametric logistic fits. (c) Relative SRB release from the cross-reactivity studies with lateral flow assay using materials **S2.3$_A$.2-B11** (orange) and **S5.3$_A$.2-B11** (blue) in the presence of 2 ppm of TATP and potentially cross-reacting compound in PBS (pH 7.4) as indicated in the graphs.

those observed in the suspension assays above. Again, a better selectivity was found for the MCM-41-type host material (Figure 7c). Selectivity studies in the presence of a mixture of explosives were not evaluated, since the parallel use of different explosives might not be the most frequent scenario. However, in our previous work,[30] we already observed that the response of these materials also showed low cross-reactivity.

The fluorescence traces along the strip shown in Figure 6a suggest that one of the factors leading to worse limits of detection might be the broadness of the signals. Several conventional strategies were thus invoked, such as the application of additional commercially available blocking, focusing, or conjugation pads, as well as the use of Tween as an auxiliary surfactant reagent or specific impregnation of the area around zone B with a PBS 10× line, but all of these had no beneficial effect on the strips' performance. On the contrary, for some of the approaches, the flow was reduced, prolonging assay times. However, when shorter strips of 0.5 × 2.5 cm were used and 0.5 μL of a suspension of **S2.3$_A$.2-B11** (2 mg mL^{-1}, Figure S16) were deposited in zone A with a micropipette, better-focused signals were obtained in a TATP assay in both, the absence (Figure S17a vs Figure 6a, black line) and the presence (Figure S17b vs Figure 6a, red line) of 500 ppb of TATP. A smaller spot in zone A produced a narrower signal in zone B. Accordingly, concentration-dependent experiments with TATP now yielded a better sensitivity as before, lowering the LOD to 9.3 ± 2.6 ppb.

Encouraged by these results, the use of an automated dispenser able to deliver droplets of ≤1 nL (Figure S18a) with respect to further performance optimization was investigated. The advantage of this procedure would be an automated and reproducible preparation of the test strips. At first, the most suitable volume to be deposited was addressed by depositing spots of 1× 10, 1× 50, 1× 100, and 1× 200 nL of **S2.3$_A$.2-B11** (5 mg mL^{-1}) on a strip of 4 cm (manual movement of the strip) and measuring the fluorescence. Figure S18b reveals that spots of ca. 1 mm diameter were obtained, with 50 nL yielding the narrowest yet most intense signal. Reproducibility

https://doi.org/10.1021/acsanm.1c03417
ACS Appl. Nano Mater. 2022, 5, 626−641

experiments were then carried out, revealing favorable results of 0.59 ± 0.01 mm full width at half-height of the fluorescence signals of nine spots deposited in a row on a strip by the dispenser (with manual strip movement). Repetition by depositing single spots of 50 nL of **S2.3$_A$.2-B11** suspensions (5 mg mL^{-1}) on various strips with the automated dispenser yielded similarly convincing results. In the next series of experiments, the amount of material deposited was screened, using suspensions of **S2.3$_A$.2-B11** of 2, 5, and 10 mg mL^{-1}. Whereas the selectivity was found to be unaltered, dye release was different, resulting in different LODs. Figure S17d depicts the response curves as a function of TATP concentration, indicating that the best LOD of 30.3 ± 4.6 ppb was found for dispensing 50 nL of suspensions of 5 mg mL^{-1} of **S2.3$_A$.2-B11**. The usage of less gAID material in the suspension led to less signal, and the usage of 10 mg mL^{-1} produced a higher signal in zone A, but the delivery of the dye was apparently aggravated, leading to a distinctly smaller ratiometric signal than for 5 mg mL^{-1} suspension.

These experiments have shown that the non-covalently capped hybrid materials are stable enough to be handled in an automated dispensing process using a piezo-driven device. In a further step to automation, suspensions of **S2.3$_A$.2-B11** were also dispensed on strips with a sciFlexarrayer S11 spotter, which allows for both fully automated dispensing and strip movement. Unfortunately, as can be seen in Figure S19, severe sedimentation problems of the particles in the reservoir were encountered. Figure S19a,b shows two strips prepared in one run from the same reservoir. It is evident that already the second spotting step produced only a 10-fold lower signal than the first. Moreover, no signal was observed for the third strip (results not shown). Only when the suspensions were stirred during strip preparation were reproducible spots obtained (Figures S19c,d). Thus, constant stirring of the suspension in the reservoir of a spotter is essential for achieving acceptable reproducibility.

In a final series of experiments, the ability of the strips to be used in a realistic scenario was evaluated, employing strips prepared through manual dispensing. The scenarios chosen were the detection of TATP in tap water (pH 7.4) and in influent (pH 7.9) as well as effluent (pH 7.5) water of a sewage treatment plant. The water samples were thus spiked with different amounts of TATP. To assess matrix effects, fractions of 0.1 mL of PBS 10× solution were added to 0.9 mL of each of the spiked samples, the strips were dipped into the samples, and the LFA was developed according to our standard protocol, employing 0.5 × 2.5 cm strips and spotting 0.5 μL (2 mg mL^{-1} **S2.3$_A$.2-B11**) at 2 mm from the bottom (see above and Figure S19, SI). Using this method, it was possible to detect TATP in tap water with a limit of detection of 40.5 ± 8.6 ppb (see Figure S20, SI). The detection of TATP in influent and effluent water from a sewage treatment plant was also evaluated, allowing a release of 9.0 ± 0.8% of dye confined in the sensing material in the presence of 5 ppm of TATP (Figure S21a,b, SI).

The pH tolerance of the immunochemical gAID system was tested in the range of pH 1−12, in the presence of 1 ppm TATP. Acidic and basic solutions were adjusted to the respective pH with either 0.25 M aqueous HCl or 0.1 M aqueous KOH solution. Subsequently, 10 μL of TATP stock solution (100 ppm) were added to 990 μL of the as-prepared pH solutions and gently shaken for 15 min at room temperature. Then, strips containing **S2.3$_A$.2-B11** were developed as described above. When TATP was present in a sample, delivery of SRB was observed at any pH. However, below pH 4 and above pH 8.5, the delivery was reduced by ca. 50 and 80%, respectively, presumably because the pH changes affect the stability of the antibodies, altering the number and distribution of charges on the protein surface,[66] and also because at acidic pH, TATP starts to decompose[67] and at alkaline pH, the structure of the silica scaffold might be altered (Figure S21c,d, SI).[68] In addition, the assay was also tested for its tolerance against a common organic solvent such as ethanol, in the range of 1−10% (v/v). The results revealed that only at >5% ethanol is the release enhanced, most likely due to accelerated dissociation of the antibody caps (Figure S21e,f, SI).

4. CONCLUSIONS

The present work described the major steps of optimizing the immunochemical recognition part of antibody-gated indicator releasing materials based on mesoporous silica nanoparticles with the example of an immunochemical TATP detection. Several iterative cycles and the tuning of various parameters have allowed us to obtain sensing materials that can be used for the determination of the peroxide-based explosive with a lateral-flow fluorescence reader in the lower ppb range without further treatment or conditioning of the test strips and fast overall assay times of <10 min. Due to the detection mechanism, a release of a much larger number of entrapped dye molecules from the pores than analyte molecules being necessary to displace the antibodies from the pore openings leads to amplification factors between 70−200 with TATP concentrations between 20−60 ppb. The choice of a slightly mismatched (heterologous) hapten (**IV**) as compared to the hapten used for immunization (**III**) enhances the performance of the materials significantly, while the type of mesoporous silica host was less decisive when choosing the right functionalization approach. Further optimization steps included capping conditions, dilution of the sera employed, the affinity of the antibodies in the sera, and the use of an organic co-solvent. In addition to favorable sensitivity, good selectivity has been observed, especially for the discrimination of TATP against H_2O_2. While the assay time could be shortened to <5 min in suspension, it takes between 3 and 8 min in the LFA format, depending on how fast the strip is dried after development.

Incorporation of the best performing gAID materials on nitrocellulose membrane strips yielded a powerful lateral-flow assay detection system. Further optimization concerning the length of strips, the amount of material, and the method of spot deposition allowed to retain the performance rather well for such a simple and easy-to-use test, which could be employed for realistic samples such as the influent and effluent of wastewater treatment plants, detecting TATP at lower ppb concentrations in such environments.

Besides simplicity and performance, the strength of such systems lies with their modularity and generalizability, being applicable for many small-molecule analytes, against which antibodies are available or can be raised and allowing for multiplexed analysis with such simple assay formats.

■ ASSOCIATED CONTENT

Supporting Information

The Supporting Information is available free of charge at https://pubs.acs.org/doi/10.1021/acsanm.1c03417.

https://doi.org/10.1021/acsanm.1c03417
ACS Appl. Nano Mater. 2022, 5, 626−641

Materials characterization, additional studies in suspension, strip preparation, additional LFA studies, limits of detection, and measurement uncertainties (PDF)

AUTHOR INFORMATION

Corresponding Author

Estela Climent − *Department Analytical Chemistry; Reference Materials, Bundesanstalt für Materialforschung und -prüfung (BAM), Berlin 12489, Germany;* orcid.org/0000-0002-6128-1235; Email: estela.climent@bam.de

Authors

Michael G. Weller − *Department Analytical Chemistry; Reference Materials, Bundesanstalt für Materialforschung und -prüfung (BAM), Berlin 12489, Germany;* orcid.org/0000-0003-2767-2029

Ramón Martínez-Máñez − *Instituto Interuniversitario de Investigación de Reconocimiento Molecular y Desarrollo Tecnológico (IDM) Universitat Politècnica de València, Universitat de València, Valencia 46022, Spain; Unidad Mixta UPV-CIPF de Investigación en Mecanismos de Enfermedades y Nanomedicina, Universitat Politècnica de València, Centro de Investigación Príncipe Felipe, Valencia 46012, Spain; CIBER de Bioingeniería, Biomateriales y Nanomedicina (CIBER-BBN), Madrid 28029, Spain;* orcid.org/0000-0001-5873-9674

Knut Rurack − *Department Analytical Chemistry; Reference Materials, Bundesanstalt für Materialforschung und -prüfung (BAM), Berlin 12489, Germany;* orcid.org/0000-0002-5589-5548

Complete contact information is available at: https://pubs.acs.org/10.1021/acsanm.1c03417

Author Contributions

Conceptualization was done by E.C. and K.R.; funding acquisition was done by E.C. and R.M.M.; investigation was done by E.C.; methodology was done by E.C., M.G.W., R.M.M., and K.R.; project administration was done by E.C.; resources were procured by E.C., M.G.W., and K.R.; supervision was done by E.C., R.M.M., and K.R.; validation was done by E.C. and K.R.; visualization was done by E.C. and K.R.; writing of the original draft was done by E.C.; and editing was done by K.R., M.G.W., and R.M.M.

Funding

This research was funded by the German Research Foundation (DFG; CL 761/1-19), the Spanish Government (project RTI2018-100910-B-C41 (MCUI/FEDER, EU)), and the Generalitat Valenciana (project PROMETEO 2018/024).

Notes

The authors declare no competing financial interest.

ACKNOWLEDGMENTS

We thank F. Sancenón and M. D. Marcos (Universitat Politècnica de València) for TGA, PXRD, and TEM measurements, P. Amorós (Universitat de València) for N_2 adsorption/desorption measurements, J. Odoj (Humboldt University Berlin) for elemental analysis, D. Pfeifer and C. Jäger (BAM, Structural Analysis Division) for NMR support, M. Hecht and D. Gröninger (BAM, Chemical and Optical Sensing Division) for support with materials screening, and M. A. Walter (BAM, Protein Analysis Division) for obtaining the sera.

ADDITIONAL NOTE

[a]Pyrethroids ELISA Kits PN 500201, PN 500204, Abraxis, Inc., Warminster, PA. The purified monoclonal mouse anti-pyrethroids (PY-1) antibody was kindly provided by Abraxis separately from the kit.

REFERENCES

(1) Ariga, K.; Vinu, A.; Hill, J. P.; Mori, T. Coordination chemistry and supramolecular chemistry in mesoporous nanospace. *Coord. Chem. Rev.* **2007**, *251*, 2562−2591.

(2) Croissant, J. G.; Fatieiev, Y.; Almalik, A.; Khashab, N. M. Mesoporous Silica and Organosilica Nanoparticles: Physical Chemistry, Biosafety, Delivery Strategies, and Biomedical Applications. *Adv. Healthcare Mater.* **2018**, *7*, 1700831.

(3) Rurack, K.; Martínez-Máñez, R., *The Supramolecular Chemistry of Organic-Inorganic Hybrid Materials*; John Wiley & Sons: Hoboken, NJ, 2010.

(4) Qiao, Y.; Wan, J.; Zhou, L.; Ma, W.; Yang, Y.; Luo, W.; Yu, Z.; Wang, H. Stimuli-responsive nanotherapeutics for precision drug delivery and cancer therapy. *Wiley Interdiscip. Rev.: Nanomed. Nanobiotechnol.* **2019**, *11*, No. e1527.

(5) Cai, H.; Wang, P.; Zhang, D. Smart anticorrosion coating based on stimuli-responsive micro/nanocontainer: a review. *J. Oceanol. Limnol.* **2020**, *38*, 1045−1063.

(6) Wang, Y.; Yan, J.; Wen, N.; Xiong, H.; Cai, S.; He, Q.; Hu, Y.; Peng, D.; Liu, Z.; Liu, Y. Metal-organic frameworks for stimuli-responsive drug delivery. *Biomaterials* **2020**, *230*, 119619.

(7) Guimaraes, R. S.; Rodrigues, C. F.; Moreira, A. F.; Correia, I. J. Overview of stimuli-responsive mesoporous organosilica nanocarriers for drug delivery. *Pharmacol. Res.* **2020**, *155*, 104742.

(8) Rahikkala, A.; Pereira, S. A. P.; Figueiredo, P.; Passos, M. L. C.; Araújo, A. R. T. S.; Saraiva, M. L. M. F. S.; Santos, H. A. Mesoporous Silica Nanoparticles for Targeted and Stimuli-Responsive Delivery of Chemotherapeutics: A Review. *Adv. Biosyst.* **2018**, *2*, 1800020.

(9) Liu, Z.; Wang, W.; Xie, R.; Ju, X. J.; Chu, L. Y. Stimuli-responsive smart gating membranes. *Chem. Soc. Rev.* **2016**, *45*, 460−475.

(10) Tao, Y.; Chan, H. F.; Shi, B.; Li, M.; Leong, K. W. Light: A Magical Tool for Controlled Drug Delivery. *Adv. Funct. Mater.* **2020**, *30*, 2005029.

(11) Poscher, V.; Salinas, Y. Trends in Degradable Mesoporous Organosilica-Based Nanomaterials for Controlling Drug Delivery: A Mini Review. *Materials* **2020**, *13*, 3668.

(12) Castillo, R. R.; Lozano, D.; González, B.; Manzano, M.; Izquierdo-Barba, I.; Vallet-Regí, M. Advances in mesoporous silica nanoparticles for targeted stimuli-responsive drug delivery: an update. *Expert Opin. Drug Delivery* **2019**, *16*, 415−439.

(13) Alejo, T.; Uson, L.; Arruebo, M. Reversible stimuli-responsive nanomaterials with on-off switching ability for biomedical applications. *J. Controlled Release* **2019**, *314*, 162−176.

(14) Li, Z.; Song, N.; Yang, Y. W. Stimuli-Responsive Drug-Delivery Systems Based on Supramolecular Nanovalves. *Matter* **2019**, *1*, 345−368.

(15) Aznar, E.; Oroval, M.; Pascual, L.; Murguía, J. R.; Martínez-Máñez, R.; Sancenón, F. Gated Materials for On-Command Release of Guest Molecules. *Chem. Rev.* **2016**, *116*, 561−718.

(16) Descalzo, A. B.; Martínez-Mañez, R.; Sancenón, R.; Hoffmann, K.; Rurack, K. The supramolecular chemistry of organic-inorganic hybrid materials. *Angew. Chem., Int. Ed.* **2006**, *45*, 5924−5948.

(17) Hofmann, C.; Duerkop, A.; Baeumner, A. J. Nanocontainers for Analytical Applications. *Angew. Chem., Int. Ed.* **2019**, *58*, 12840−12860.

(18) Martínez-Mañez, R.; Sancenón, F.; Biyikal, M.; Hecht, M.; Rurack, K. Mimicking tricks from nature with sensory organic-inorganic hybrid materials. *J. Mater. Chem.* **2011**, *21*, 12588−12604.

(19) Hecht, M.; Climent, E.; Biyikal, M.; Sancenón, F.; Martínez-Mañez, R.; Rurack, K. Gated hybrid delivery systems: En route to sensory materials with inherent signal amplification. *Coord. Chem. Rev.* **2013**, *257*, 2589−2606.

(20) Sancenón, F.; Pascual, L.; Oroval, M.; Aznar, E.; Martínez-Máñez, R. Gated Silica Mesoporous Materials in Sensing Applications. *ChemistryOpen* **2015**, *4*, 418−437.
(21) Climent, E.; Marcos, M. D.; Martínez-Máñez, R.; Sancenón, F.; Soto, J.; Rurack, K.; Amorós, P. The Determination of Methylmercury in Real Samples Using Organically Capped Mesoporous Inorganic Materials Capable of Signal Amplification. *Angew. Chem., Int. Ed.* **2009**, *48*, 8519−8522.
(22) Climent, E.; Mondragón, L.; Martínez-Mañez, R.; Sancenón, F.; Marcos, M. D.; Murguia, J. R.; Amorós, P.; Rurack, K.; Pérez-Payá, E. Selective, Highly Sensitive, and Rapid Detection of Genomic DNA by Using Gated Materials: Mycoplasma Detection. *Angew. Chem., Int. Ed.* **2013**, *52*, 8938−8942.
(23) Giménez, C.; Climent, E.; Aznar, E.; Martínez-Mañez, R.; Sancenón, F.; Marcos, M. D.; Amorós, P.; Rurack, K. Towards Chemical Communication between Gated Nanoparticles. *Angew. Chem., Int. Ed.* **2014**, *53*, 12629−12633.
(24) Bell, J.; Climent, E.; Hecht, M.; Buurman, M.; Rurack, K. Combining a Droplet-Based Microfluidic Tubing System with Gated Indicator Releasing Nanoparticles for Mercury Trace Detection. *ACS Sens.* **2016**, *1*, 334−338.
(25) Climent, E.; Bernardos, A.; Martínez-Mañez, R.; Maquieira, A.; Marcos, M. D.; Pastor-Navarro, N.; Puchades, R.; Sancenón, F.; Soto, J.; Amorós, P. Controlled Delivery Systems Using Antibody-Capped Mesoporous Nanocontainers. *J. Am. Chem. Soc.* **2009**, *131*, 14075−14080.
(26) Climent, E.; Martinez-Manez, R.; Maquieira, A.; Sancenon, F.; Marcos, M. D.; Brun, E. M.; Soto, J.; Amoros, P. Antibody-Capped Mesoporous Nanoscopic Materials: Design of a Probe for the Selective Chromo-Fluorogenic Detection of Finasteride. *ChemistryOpen* **2012**, *1*, 251−259.
(27) Climent, E.; Gröninger, D.; Hecht, M.; Walter, M. A.; Martínez-Mañez, R.; Weller, M. G.; Sancenon, F.; Amorós, P.; Rurack, K. Selective, Sensitive, and Rapid Analysis with Lateral-Flow Assays Based on Antibody-Gated Dye-Delivery Systems: The Example of Triacetone Triperoxide. *Chem. − Eur. J.* **2013**, *19*, 4117−4122.
(28) Costa, E.; Climent, E.; Ast, S.; Weller, M. G.; Canning, J.; Rurack, K. Development of a lateral flow test for rapid pyrethroid detection using antibody-gated indicator-releasing hybrid materials. *Analyst* **2020**, *145*, 3490−3494.
(29) Costa, E.; Climent, E.; Gawlitza, K.; Wan, W.; Weller, M. G.; Rurack, K. Optimization of analytical assay performance of antibody-gated indicator-releasing mesoporous silica particles. *J. Mater. Chem. B* **2020**, *8*, 4950−4961.
(30) Climent, E.; Biyikal, M.; Gröninger, D.; Weller, M. G.; Martínez-Máñez, R.; Rurack, K. Multiplexed Detection of Analytes on Single Test Strips with Antibody-Gated Indicator-Releasing Mesoporous Nanoparticles. *Angew. Chem., Int. Ed.* **2020**, *59*, 23862−23869.
(31) Pla, L.; Santiago-Felipe, S.; Tormo-Mas, M. Á.; Pemán, J.; Sancenón, F.; Aznar, E.; Martínez-Máñez, R. Aptamer-Capped nanoporous anodic alumina for Staphylococcus aureus detection. *Sens. Actuators, B* **2020**, *320*, 128281.
(32) Zheng, Z.; Huang, X.; Schenderlein, M.; Moehwald, H.; Xu, G. K.; Shchukin, D. G. Bioinspired nanovalves with selective permeability and pH sensitivity. *Nanoscale* **2015**, *7*, 2409−2416.
(33) Gisbert-Garzarán, M.; Vallet-Regí, M. Influence of the Surface Functionalization on the Fate and Performance of Mesoporous Silica Nanoparticles. *Nanomaterials* **2020**, *10*, 916.
(34) Wang, J.; Ma, Q.; Wang, Y.; Li, Z.; Li, Z.; Yuan, Q. New insights into the structure-performance relationships of mesoporous materials in analytical science. *Chem. Soc. Rev.* **2018**, *47*, 8766−8803.
(35) Zhao, D.; Wan, Y.; Zhou, W., Representative Mesoporous Silica Molecular Sieves. In *Ordered Mesoporous Materials*; Zhao, D.; Wan, Y.; Zhou, W., Eds. Wiley-VCH: Weinheim, 2013; pp. 153−217.
(36) Climent, E.; Hecht, M.; Rurack, K. Loading and Release of Charged and Neutral Fluorescent Dyes into and from Mesoporous Materials: A Key Role for Sensing Applications. *Micromachines* **2021**, *12*, 249.
(37) Stanker, L. H.; Bigbee, C.; Van Emon, J.; Watkins, B.; Jensen, R. H.; Morris, C.; Vanderlaan, M. An Immunoassay for Pyrethroids - Detection of Permethrin in Meat. *J. Agric. Food Chem.* **1989**, *37*, 834−839.
(38) Chuang, J. C.; Van Emon, J. M.; Tefft, M. E.; Wilson, N. K. Application of a permethrin immunosorbent assay method to residential soil and dust samples. *J. Environ. Sci. Health, Part B* **2010**, *45*, 516−523.
(39) Walter, M. A.; Pfeifer, D.; Kraus, W.; Emmerling, F.; Schneider, R. J.; Panne, U.; Weller, M. G. Triacetone Triperoxide (TATP): Hapten Design and Development of Antibodies. *Langmuir* **2010**, *26*, 15418−15423.
(40) Walter, M. A.; Panne, U.; Weller, M. G. A Novel Immunoreagent for the Specific and Sensitive Detection of the Explosive Triacetone Triperoxide (TATP). *Biosensors* **2011**, *1*, 93.
(41) Ramin, S.; Weller, M. G. Extremely sensitive and selective antibodies against the explosive 2,4,6-trinitrotoluene by rational design of a structurally optimized hapten. *J. Mol. Recognit.* **2012**, *25*, 89−97.
(42) Hesse, A.; Biyikal, M.; Rurack, K.; Weller, M. G. Development of highly sensitive and selective antibodies for the detection of the explosive pentaerythritol tetranitrate (PETN) by bioisosteric replacement. *J. Mol. Recognit.* **2016**, *29*, 88−94.
(43) Burks, R. M.; Hage, D. S. Current trends in the detection of peroxide-based explosives. *Anal. Bioanal. Chem.* **2009**, *395*, 301−313.
(44) To, K. C.; Ben-Jaber, S.; Parkin, I. P. Recent Developments in the Field of Explosive Trace Detection. *ACS Nano* **2020**, *14*, 10804−10833.
(45) Dubnikova, F.; Kosloff, R.; Almog, J.; Zeiri, Y.; Boese, R.; Itzhaky, H.; Alt, A.; Keinan, E. Decomposition of Triacetone Triperoxide Is an Entropic Explosion. *J. Am. Chem. Soc.* **2005**, *127*, 1146−1159.
(46) Wierzbicki, A.; Cioffi, E. Density Functional Theory Studies of Hexamethylene Triperoxide Diamine. *J. Phys. Chem. A* **1999**, *103*, 8890−8894.
(47) Langone, J. J.; Vanvunakis, H., [48] Radioimmunoassay of nicotine, cotinine, and γ3-Pyridyl-γ-oxo-N-methylbutyramidle. In *Methods in Enzymology*; Academic Press: 1982; Vol. *84*, pp. 628−640.
(48) Kresge, C. T.; Leonowicz, M. E.; Roth, W. J.; Vartuli, J. C.; Beck, J. S. Ordered mesoporous molecular sieves synthesized by a liquid-crystal template mechanism. *Nature* **1992**, *359*, 710−712.
(49) Radu, D. R.; Lai, C.-Y.; Jeftinija, K.; Rowe, E. W.; Jeftinija, S.; Lin, V. S. Y. A Polyamidoamine Dendrimer-Capped Mesoporous Silica Nanosphere-Based Gene Transfection Reagent. *J. Am. Chem. Soc.* **2004**, *126*, 13216−13217.
(50) Zhao, D.; Feng, J.; Huo, Q.; Melosh, N.; Fredrickson, G. H.; Chmelka, B. F.; Stucky, G. D. Triblock Copolymer Syntheses of Mesoporous Silica with Periodic 50 to 300 Angstrom Pores. *Science* **1998**, *279*, 548−552.
(51) Climent, E.; Biyikal, M.; Gawlitza, K.; Dropa, T.; Urban, M.; Costero, A. M.; Martínez-Máñez, R.; Rurack, K. Determination of the chemical warfare agents Sarin, Soman and Tabun in natural waters employing fluorescent hybrid silica materials. *Sens. Actuators, B* **2017**, *246*, 1056−1065.
(52) Sathe, M.; Derveni, M.; Broadbent, G.; Bodlenner, A.; Charlton, K.; Ravi, B.; Rohmer, M.; Sims, M. R.; Cullen, D. C. Synthesis and characterisation of immunogens for the production of antibodies against small hydrophobic molecules with biosignature properties. *Anal. Chim. Acta* **2011**, *708*, 97−106.
(53) Goodrow, M. H.; Hammock, B. D. Hapten design for compound-selective antibodies: ELISAS for environmentally deleterious small molecules. *Anal. Chim. Acta* **1998**, *376*, 83−91.
(54) Pryde, D. C.; Jones, L. H.; Gervais, D. P.; Stead, D. R.; Blakemore, D. C.; Selby, M. D.; Brown, A. D.; Coe, J. W.; Badland, M.; Beal, D. M.; Glen, R.; Wharton, Y.; Miller, G. J.; White, P.; Zhang, N.; Benoit, M.; Robertson, K.; Merson, J. R.; Davis, H. L.; McCluskie, M. J. Selection of a Novel Anti-Nicotine Vaccine: Influence of Antigen Design on Antibody Function in Mice. *PLoS One* **2013**, *8*, No. e76557.

https://doi.org/10.1021/acsanm.1c03417
ACS Appl. Nano Mater. 2022, 5, 626−641

(55) Ceballos-Alcantarilla, E.; López-Puertollano, D.; Agulló, C.; Abad-Fuentes, A.; Abad-Somovilla, A.; Mercader, J. V. Combined heterologies for monoclonal antibody-based immunoanalysis of fluxapyroxad. *Analyst* **2018**, *143*, 5718−5727.
(56) Kim, Y. J.; Cho, Y. A.; Lee, H.-S.; Lee, Y. T.; Gee, S. J.; Hammock, B. D. Synthesis of haptens for immunoassay of organophosphorus pesticides and effect of heterology in hapten spacer arm length on immunoassay sensitivity. *Anal. Chim. Acta* **2003**, *475*, 85−96.
(57) Piran, U.; Silbert-Shostek, D.; Barlow, E. H. Role of antibody valency in hapten-heterologous immunoassays. *Clin. Chem.* **1993**, *39*, 879−883.
(58) Tamarit-López, J.; Morais, S.; Bañuls, M.-J.; Puchades, R.; Maquieira, Á. Development of Hapten-Linked Microimmunoassays on Polycarbonate Discs. *Anal. Chem.* **2010**, *82*, 1954−1963.
(59) Zhang, Q.; Wang, L.; Ahn, K. C.; Sun, Q.; Hu, B.; Wang, J.; Liu, F. Hapten heterology for a specific and sensitive indirect enzyme-linked immunosorbent assay for organophosphorus insecticide fenthion. *Anal. Chim. Acta* **2007**, *596*, 303−311.
(60) Climent, E.; Hecht, M.; Witthuhn, H.; Gawlitza, K.; Rurack, K. Mix-&-Read Determination of Mercury(II) at Trace Levels with Hybrid Mesoporous Silica Materials Incorporating Fluorescent Probes by a Simple Mix-&-Load Technique. *ChemistryOpen* **2018**, *7*, 957−968.
(61) Russell, A. J.; Trudel, L. J.; Skipper, P. L.; Groopman, J. D.; Tannenbaum, S. R.; Klibanov, A. M. Antibody-antigen binding in organic solvents. *Biochem. Biophys. Res. Commun.* **1989**, *158*, 80−85.
(62) Lou, X.; Zhu, A.; Luo, Q.; Zhang, Y.; Long, F. Effects of organic solvents on immunosensing assays for small molecules based on an optofluidic immunosensing platform. *Anal. Methods* **2017**, *9*, 5731−5740.
(63) Zeck, A.; Eikenberg, A.; Weller, M. G.; Niessner, R. Highly sensitive immunoassay based on a monoclonal antibody specific for [4-arginine]microcystins. *Anal. Chim. Acta* **2001**, *441*, 1−13.
(64) Comes, M.; Marcos, M. D.; Martínez-Máñez, R.; Millán, M. C.; Ros-Lis, J. V.; Sancenón, F.; Soto, J.; Villaescusa, L. A. Anchoring Dyes into Multidimensional Large-Pore Zeolites: A Prospective Use as Chromogenic Sensing Materials. *Chem. − Eur. J.* **2006**, *12*, 2162−2170.
(65) Ros-Lis, J. V.; Casasús, R.; Comes, M.; Coll, C.; Marcos, M. D.; Martínez-Máñez, R.; Sancenón, F.; Soto, J.; Amorós, P.; El Haskouri, J.; Garró, N.; Rurack, K. A Mesoporous 3D Hybrid Material with Dual Functionality for Hg2+ Detection and Adsorption. *Chem. − Eur. J.* **2008**, *14*, 8267−8278.
(66) Wang, W.; Singh, S.; Zeng, D. L.; King, K.; Nema, S. Antibody structure, instability, and formulation. *J. Pharm. Sci.* **2007**, *96*, 1−26.
(67) Lin, H.; Suslick, K. S. A Colorimetric Sensor Array for Detection of Triacetone Triperoxide Vapor. *J. Am. Chem. Soc.* **2010**, *132*, 15519−15521.
(68) Pham, A. L.-T.; Sedlak, D. L.; Doyle, F. M. Dissolution of Mesoporous Silica Supports in Aqueous Solutions: Implications for Mesoporous Silica-based Water Treatment Processes. *Appl Catal B* **2012**, *126*, 258−264.

https://doi.org/10.1021/acsanm.1c03417
ACS Appl. Nano Mater. 2022, 5, 626−641